Bridging Adsorption Analytics and Catalytic Kinetics for Metal-Exchanged Zeolites

Pengfei Xie
Johns Hopkins University https://orcid.org/0000-0002-7644-9934
Tiancheng Pu
Johns Hopkins University
Gregory Aranovich
Johns Hopkins University
Jiawei Guo
University of California, Davis
Marc Donohue
Johns Hopkins University
Ambarish Kulkarni
University of California, Davis
Chao Wang (chaowang@jhu.edu)
Johns Hopkins University https://orcid.org/0000-0001-7398-2090

Article

Keywords: adsorption compression, NO decomposition, copper-exchanged zeolites, kinetics

Posted Date: September 3rd, 2020

DOI: https://doi.org/10.21203/rs.3.rs-63384/v1

Version of Record: A version of this preprint was published at Nature Catalysis on February 1st, 2021. See the published version at https://doi.org/10.1038/s41929-020-00555-0.

Bridging Adsorption Analytics and Catalytic Kinetics for Metal-Exchanged Zeolites

Pengfei Xie,[1] Tiancheng Pu,[1] Gregory Aranovich,[1] Jiawei Guo,[2] Marc Donohue,[1] Ambarish Kulkarni,[2,] Chao Wang[1,]**

[1] Department of Chemical and Biomolecular Engineering, Johns Hopkins University, Baltimore, Maryland 21218, United States

[2] Department of Chemical Engineering, University of California, Davis, California 95616, United States

KEYWORDS: *adsorption compression, NO decomposition, copper-exchanged zeolites, kinetics*

Abstract.

Metal-exchanged zeolites have been widely used in industrial catalysis and separation, but fundamental understanding of their structure-property relationships has remained challenging, largely due to the lack of quantitative information concerning the atomic structures and reaction-relevant adsorption properties of the embedded metal active sites. We report on the use of low-temperature chemisorption to titrate Cu-exchanged ZSM5. Quantitative descriptors of the atomic structures and adsorption properties of Cu-ZSM5 are established by combining atomistic simulation, DFT calculations, operando molecular spectroscopy, chemisorption and titration measurements. These descriptors are then applied to interpret the catalytic performance of Cu-ZSM5 for NO decomposition. Linear correlations are established to bridge the low-temperature adsorption analytics and high-temperature reaction kinetics, which are demonstrated to be generally applicable for understanding the structure-property relationships of metal exchanged zeolites and foregrounded for guiding the development of advanced catalytic materials.

INTRODUCTION

Portraiture of active sites and their adsorption properties represents a grand challenge but utmost task for the development of advanced catalysts. Conventionally it largely relies on microscopic and spectroscopic techniques to characterize the structures of catalytic materials and probe reaction-relevant adsorbates, respectively.[1,2] These approaches are, however, either limited by the insensitivity to the active sites on catalyst surfaces (e.g., for transmission electron microscopy, TEM[2] and X-ray absorption spectroscopy, XAS[3]), or subject to the rendered signal-to-noise ratios at elevated reaction temperatures and inadequacy of acquiring quantitative information (such as infrared[4] and Raman[5] spectroscopy). On the other hand, computational approaches such as density functional theory (DFT) calculations are extensively used to simulate reaction pathways and understand catalytic mechanisms, with energetics of adsorbing intermediates commonly established as descriptors to understand the trends of kinetic performance and guide catalyst designs.[6,7] But such calculations usually require pre-established structure models of catalytic materials and quantitative validation of the computed structure-property relationships are nontrivial in experiments.

Direct decomposition of NO to N_2 and O_2 is the most robust strategy for NO removal from combustion emissions, as it does not rely on the presence or addition of reductants to the exhaust stream.[8,9] Cu-ZSM5 represents a promising and extensively studied catalyst for this reaction. Both isolated monomeric[10-13] and associated dimeric[14-17] Cu sites have been discussed as the active sites. The Cu dimers in Cu-ZSM5 have been probed by using various spectroscopic techniques, including ultraviolet–visible spectroscopy (UV-Vis),[18-20] Fourier-transform infrared spectroscopy (FTIR),[20-25] resonance Raman spectroscopy (Raman),[26,27] electron paramagnetic resonance (EPR)[28-30] and XAS[21,31-33]. Computational studies also support the formation of dicopper-oxo

centers ($[Cu\text{-}O\text{-}Cu]^{2+}$) when NO_x (NO[34,35] or N_2O[36]) interacts with Cu-ZSM5. Albeit the abundant evidence for their formation and involvement in the NO decomposition reaction, quantitative characterization of the Cu-dimer motifs remains largely challenging. The overall low population and small coordination number (up to CN = 1 for Cu···Cu coordination if all the Cu sites are in dimeric configurations such as $[Cu\text{-}O\text{-}Cu]^{2+}$) of Cu sites cause large uncertainties in the assignment of the second-shell feature in EXAFS spectra.[31,32] Temperature-programmed reaction (TPR) measurements have been reported to quantify Cu dimers in oxygen-pretreated Cu-ZSM5 of a fixed Si/Al ratio with different Cu exchange levels, but it remains elusive whether this means is generally applicable.[37] Such measurements are also limited due to the inability of obtaining reaction-relevant structure information and adsorption properties, due to the different chemical conditions (e.g., O_2 vs. NO_x) involved in TPR as compared to the catalytic process. Similar challenges are also present for other metal-exchanged zeolites that are of broad interests in catalysis and separation.[38-42]

We report here the use of reactive adsorption to titrate the atomic structures and adsorption properties of metal-exchanged zeolites. On the basis of a series of Cu-exchanged ZSM5 with different Si/Al ratios but all at full exchange, we first performed atomistic simulations to quantify the Cu dimers within the pentasil framework, and conducted temperature-programmed reaction (TPR) measurements to validate the predicted descriptor. We then combined DFT calculations, diffuse reflectance infrared Fourier transform spectroscopy (DRIFTS) and chromatographic titration of gaseous effluents to evaluate the low-temperature interaction of NO with the series of Cu-ZSM5. Reaction-relevant adsorption analytics were derived to establish correlations between the atomic structures and adsorption properties of the Cu sites, which were then employed to interpret the kinetics of NO decomposition catalyzed by Cu-ZSM5. We further generalized these relationships to understand the structure-performance correlations for other types of zeolites in NO

decomposition and also for Cu-ZSM5 in catalyzing methane-to-methanol (MTM) conversion. Our work aims to excel the bridge between low-temperature adsorption analytics and high-temperature reaction kinetics in heterogeneous catalysis.

RESULTS AND DISCUSSION

Synthesis of Cu-ZSM5. We first prepared a series of pristine ZSM5 with different Si/Al ratios (11.5, 20, 30, 50 and 100, as determined by X-ray fluorescence (XRF) spectroscopy) by using hydrothermal synthesis.[43,44] The as-synthesized ZSM5 exhibits a rectangular parallelepiped shape with the over particle size in the micrometer scale (Figure S1). They were converted into Na-type and then Na^+ was substituted with Cu^{2+} via ion exchange (see the Experimental Method).[45,46] A Cu/Al ratio of ~0.5 was targeted for full exchange (Table 1).[46] In the following discussion, the Cu-exchanged zeolites are denoted as Cu-ZSM5-*x*, where *x* represents the Si/Al element ratio, e.g., Cu-ZSM5-11.5 for Cu-ZSM5 with Si/Al ~ 11.5. Brunauer–Emmett–Teller (BET) measurements show that the five types of Cu-ZSM5 have rather consistent specific surface areas in the range of 370–400 $m^2\ g^{-1}$ (Table 1, also see Figure S2 for the N_2 adsorption and desorption isotherms).[44,47] X-ray diffraction (XRD) patterns collected on the Cu-ZSM5 catalysts exhibit peaks corresponding to the MFI phase (JCDPS No. 37-0359) but not for copper oxides (Cu_2O or CuO), indicating that the Cu species are highly dispersed in the zeolites (Figure S3).

For studying the interaction with NO, the Cu-ZSM5 catalysts were pretreated in He at 500 ^oC. Post the activation the Cu species in Cu-ZSM5 can be present either as monomers ($[Cu^+]$) or in a dimeric configuration $[Cu^+\cdots Cu^+]$ via a so-called "auto-reduction" process,[22,31,32,35,48] with the charges balanced by one or two proximal Al centers in the framework, respectively (Figures 1a and 1b).[48-50] This was confirmed by using DRIFTS analysis to track the hydroxyl (O-H) and

framework features during the pretreatment in He (Figure S4). For the Cu dimers, it has been suggested that they are accommodated within the 10-membered ring of ZSM5 and associated with two Al sites separated by one (1T) or two (2T) -SiO_4- tetrahedra units by following the Löwenstein's rule.[40, 57, 60] Cu density in the five types of Cu-ZSM5 varies with the Si/Al ratio, decreasing from 0.52×10^{-3} $Å^{-3}$ for Cu-ZSM5-11.5 to 0.08×10^{-3} $Å^{-3}$ for Cu-ZSM5-100 (Table 1 and Figure 1c). These values correspond to a nearly linear increase of the average distance between neighboring Cu sites from 15.4 to 28.8 Å. Note that "Cu density" here refers to the average number of copper sites per unit volume of the zeolite pore, with the latter determined by BET measurements (Table 1 and Figure S2). "Average Cu···Cu distance" is determined from the "Cu density" by assuming a cubic occupation of the Cu atoms within the unit pore volume, which is different from the actual distance between neighboring Cu sites to be discussed below.[51] Previously Schoonheydt and Solomon *et al.* [26,32,36] have used XAS, UV-vis, Raman and DFT to determine the geometry of dimeric Cu motifs in Cu-ZSM5, showing Cu···Cu distances of 2.5-4.2 Å and ∠Cu−O−Cu ≈ 140°. Nonetheless, it remains challenging to quantify the atomic fractions of Cu dimers ($\eta_{Cu\cdots Cu}$, namely the percentage of Cu atoms being in dimeric configuration) within Cu-ZSM5 and characterize reaction-relevant adsorbing intermediates by using these methods.

The five types of Cu-ZSM5 form a platform with consistent framework but varying atomic structures of Cu sites. Upon the interaction with NO, Cu^{+} can be oxidized to Cu^{2+}, which is associated with structural transformation of the Cu sites, e.g., formation of oxo-copper centers, and adsorbing nitrogen oxide species. Analysis of these adsorbates thus provides a viable approach toward quantitative titration of $\eta_{Cu\cdots Cu}$ and adsorption properties for the metal-exchanged zeolite catalysts.

Fractions of Cu Dimers within Cu-ZSM5. To quantify the fraction of dimer species within the Cu-ZSM5 of various Si/Al ratios, we first performed high-throughput periodic DFT calculations (PBE functional, Grimme D3(BJ) vdW corrections, 500 eV plane wave cutoff, Γ-point only, implemented in Vienna ab-initio Simulation Package (VASP)) to calculate the formation energy of all unique $[Cu\text{-}O\text{-}Cu]^{2+}$ dimer configurations for the MFI topology. Specifically, for each inequivalent T site position for Al (12 total unique T sites for MFI, Table S1 and S2), we systematically replaced every T atom by Al within a threshold distance of 9.0 Å, resulting in a database of 167 structures (Si/Al = 47, 115 unique configurations). For each of these structures, we calculated dimer formation energies using

$$Z`Cu + Z``Cu + 0.5\ O_2 \rightarrow Z`[Cu\text{-}O\text{-}Cu]Z`` + Z_{Si} \quad (1)$$

where, Z` and Z`` represent one Al substitution in the MFI framework and $Z_{Si}$ represents the energy of an all-silica MFI framework. Although direct comparison of various Z`[Cu-O-Cu]Z`` configurations is possible (Figure S5), equation (1) allows for separate analysis of the stability of $[CuOCu]^{2+}$ motifs (which depends on reaction conditions and the oxygen chemical potential) and the underlying Al-distribution (which likely depends on the synthesis conditions). The choice of O_2 gas phase reference is motivated by the previous work.[52-57] Figure 2a summarizes the distribution of calculated dimer formation energies, with the wide span (> 2.5 eV) likely due to the favorable formation of dimers from certain Al-site pairs. Moreover, Figure 2b shows that, although dimers accommodated by the Al pairs separated with one (orange) silicon atom are on average more favorable (dotted lines, Figure 2b), certain configurations (see insets in Figure 2b) separated with two (green) or three Si atoms (red) are also very stable. The formation energies are summarized in Tables S1 and S2 and the optimized periodic structures are provided as an Atomic Simulation Environment database file[58] (ase db) in the Supplementary Information.

As the fraction of dimers formed for a given Si/Al ratio will depend on the proximity and distribution of Al atoms, we used Monte Carlo simulations to create ensembles of structures corresponding to various Si/Al ratios to obtain a statistical sampling of the relative Al locations. As the Al-siting in MFI depends on the synthesis conditions and is still widely debated,[59-61] we chose to determine the Al distribution using DFT. Specifically, we consider two extremes in Figure 2c: *i)* the Al distribution is completely determined by DFT calculated thermodynamics of Al substitution (i.e., Boltzmann-weighted) and *ii)* thermodynamics are not relevant and Al distributes randomly. In conjunction with the dimer formation energies in Figure 2b and after incorporation of entropic effects, these ensembles of Al distributions are used to estimate $\eta_{Cu\cdots Cu}$ for each Si/Al ratio at 80 °C (the temperature used in our titration experiments; see the Experimental Method). Realizing that some Al atoms are capable of stabilizing $[CuOCu]^{2+}$ dimers with multiple other Al atoms (especially at low Si/Al ratios), we populate the Al sites by starting with the most favorable $[CuOCu]^{2+}$ dimer configurations. Once an Al pair is assigned with a Cu dimer, the two Al atoms are excluded from further assignment of less stable dimers. Using this approach, the value of $\eta_{Cu\cdots Cu}$ predicted according to the Boltzmann-weighted distribution (case *i)*) varies from 0.79 for Cu-ZSM5-11.5 to 0.20 for Cu-ZSM5-100. In general, the Boltzmann-weighted distribution of Al atoms gives an approximately 20-30% higher $\eta_{Cu\cdots Cu}$ than the random Al distribution (case *ii)*). More broadly, the calculated $\eta_{Cu\cdots Cu}$ based on both Boltzmann and random distributions exhibits nearly linear dependence on the average Cu site density (Figure 2d). This correlation confirms that our simulation captures the higher tendency of forming Cu dimers for lower Si/Al ratios due to the closer proximity of Al atoms. As also shown in Figures 2c and d, $\eta_{Cu\cdots Cu}$ has a non-liner dependence on the Si/Al ratio. Results for other temperatures (Figure S6) indicate that, although the fraction of dimers reduces slightly at higher temperatures, the overall trends remain the same

as the $[CuOCu]^{2+}$ dimer can be stabilized by multiple types of Al pairs. This suggests that the MFI topology is favorable for formation of dimers, and as we will show later, low-temperature adsorption measurements can be used to probe the active sites relevant to high-temperature reactivities.

Although Cu-ZSM5 has been extensively studied, only a few reports are present for experimental quantification of the Cu dimer fractions. Iglesia *et al.*[37] used CO/H_2-TPR to evaluate $\eta_{Cu\cdots Cu}$ in Cu-ZSM5 with Si/Al = ~13-14 and Cu/Al = 0.12~0.6, and derived $\eta_{Cu\cdots Cu} \sim 44\%$, 60%, and 70% for Cu-ZSM5 with Cu/Al = 0.12, 0.38, 0.58 respectively. Owing to the limited follow-up studies using this method, its general applicability is still to be demonstrated. Moreover, CO/H_2-TPR cannot provide information about the atomic structures and adsorption properties that are pertinent to the catalytic applications (e.g., in the presence of $*NO_x$ for NO decomposition and SCR). Moretti *et al.*[35] combined irreversible CO adsorption at 298 K and N_2 adsorption at 273 K to evaluate the abundance of Cu dimers in Cu-ZSM5 by assuming strong and selective adsorption of N_2 on Cu dimers. But this method was later on questioned by Itadani *et al.*[62], who studied N_2 adsorption on Cu-MFI using a series of spectroscopic methods, including photoluminescence, X-ray absorption and infrared, and concluded with selective adsorption of N_2 on monomeric Cu^+, rather than Cu dimers. Henriques *et al.*[63] attempted to use EPR measurements to obtain *quasi*-quantitative information of the atomic structures of Cu sites within Cu-ZSM5, but debates are present on the corresponding peak assignments.[28] We have performed CO/H_2-TPR measurements on the series of Cu-ZSM5-*x* with pretreatment in oxygen (*i.e.*, 500 °C for ca. 2 h, to induce the formation of $[Cu\text{-}O\text{-}Cu]^{2+}$ centers) (Figure S7 and Table S3). Figure 2d summarizes the data collected from both the literature[37] and our own CO/H_2-TPR measurements with similar pretreatments. The results largely resemble the linear relationship correlating the $\eta_{Cu\cdots Cu}$

calculated based on the Boltzmann distribution and dimer formation via eq. (1) to the average Cu site density. The fact that our predictions are in close agreement with these experiments does not only validate the predicted distribution and structures of Cu sites, but also suggests that the established linear scaling relationship is intrinsic to the zeolite supported metal sites. The initial Boltzmann Al distributions are obtained using only the energetics of substituting a single Si atom by a single Al (with the most favorable Bronsted H location, Table S1). While the existing Al atoms may influence the siting of the other Al, such analyses are beyond the scope of this work. While not discussed here, we note that the above Monte Carlo approach can be extended based on the experimentally-determined Al positions that are influenced by kinetic factors. Moreover, we acknowledge that migration of Al sites is also possible during the oxidative pretreatment and the process of Cu dimer formation.[53,64]

Reactive Adsorption of NO on Cu-ZSM5. As noted, the $\eta_{Cu\cdots Cu}$ evaluated using CO/H_2-TPR cannot be directly related to the active sites involved in the NO decomposition reaction. This is due to the dissimilar formation energies of dicopper-oxo centers upon exposure to different oxidants (e.g., O_2, H_2O_2 and N_2O).[19,27,65,66] To merge this gap, we turned to evaluate the reactive adsorption of NO on Cu-ZSM5, aiming at probing the structure and property of the Cu sites under reaction-relevant environments. We also started with calculations of free energies for the various nitrogenous adsorbates and reaction barriers possibly involved in the interaction between NO and the Cu sites (using nudged-elastic band and dimer method). Consistent with the previously reported approaches,[67-70] the simulation was primarily applied to 1T and 2T site models (Figure 3a). A more extensive analysis by applying ensemble average to the comprehensive set of data presented in Figure 2 is currently underway and will be reported in a separate study. NO decomposition on the [$Cu^+\cdots Cu^+$] dimer sites involves three barriers related to bending of the NO

molecule (TS1), cleaving of the first N-O bond to form the $[Cu\text{-}O\text{-}Cu]^{2+}$ dimer (TS2) and reaction of N_2O with the $[Cu\text{-}O\text{-}Cu]^{2+}$ dimer for O_2 formation (TS3), where the barrier TS3 (1.6 eV, Figure 3b and 3c) likely inaccessible at 80 °C (rate ~ 10^{-10} s^{-1}). Moreover, the single NO bound state NO-$[Cu\text{-}O\text{-}Cu]^{2+}$ (blue, Figure 3d) is predicted to be most favorable at relatively low temperatures (e.g., below 100 ºC), although binding of N_2O (black) or a second NO (orange, Figure 3e) is within 0.2 eV. Finally, the reaction of desorbed N_2O with a second $[Cu^{+}\cdots Cu^{+}]$ site is favorable and results in the formation of N_2 (see Figure S8 and Scheme S1 and the Supplementary Information for details of reaction mechanism and calculated atomic structures of the intermediates based on DFT).

To validate the predicted reaction pathway, we have used diffuse reflectance infrared Fourier transform spectroscopy (DRIFTS) to characterize the stable adsorbates formed on Cu-ZSM5 upon interaction with NO. Figure 4a presents the time-dependent spectra collected on Cu-ZSM5-11.5 under the flow of 1500 ppm NO at 80 ºC (see the temporal profiles for the other four zeolites in Figure S9). Figures 4b and 4c show comparisons of the spectra recorded on Cu-ZSM5-11.5 with different partial pressures of NO (P_{NO}) and on different Cu-ZSM5 with 1500 ppm of NO, respectively (all at 15 min, see Figures S10 and S11 for more comprehensive comparisons). The corresponding peak assignments are summarized in Table S4.

The spectra recorded on Cu-ZSM5-11.5 are featured with two peaks located at 1903 and 1813 cm^{-1}. Intensities of these two peaks exhibit an inverse relationship in the dependence of time before saturation was reached at ~15 min (Figures 4d and S12). As reported by Beutel *et al.*,[22] this behavior can be attributed to the oxidation of Cu^{+} and formation of dicopper-oxo centers via the following reactions, rationalized by the measured slope of -1, assuming that extinction coefficients of NO on Cu^{+} and Cu^{2+} are similar :

$$[Cu^{+}\cdots Cu^{+}] + 2NO \rightarrow [(ON)Cu^{+}\cdots Cu^{+}(NO)] \quad (2)$$

$$[(ON)Cu^{+}\cdots Cu^{+}(NO)] \rightarrow [Cu\text{-}O\text{-}Cu]^{2+} + N_2O \quad (3)$$

$$[Cu\text{-}O\text{-}Cu]^{2+} + NO \rightarrow NO\text{-}[Cu\text{-}O\text{-}Cu]^{2+} \quad (4)$$

$$NO\text{-}[Cu\text{-}O\text{-}Cu]^{2+} + NO \rightarrow [(NO)Cu\text{-}O\text{-}Cu(NO)]^{2+} \quad (5)$$

where the transition from the 1813 cm^{-1} peak to 1903 cm^{-1} indicates the conversion of $[(ON)Cu^{+}\cdots Cu^{+}(NO)]$ to one or two NO molecules bound to $[Cu\text{-}O\text{-}Cu]^{2+}$. Our assignment is further corroborated by the DRIFTS spectra collected at saturation (15 min) under p_{NO} (Figure 4b). As P_{NO} is increased from 300 to 1500 ppm, the intensity of the 1813 cm^{-1} peak diminishes, whereas that for the 1903 cm^{-1} peak grows (Figure S13). Similar to the temporal response, this transition with p_{NO} is also associated with the transformation from $[(ON)Cu^{+}\cdots Cu^{+}(NO)]$ to $NO\text{-}[Cu\text{-}O\text{-}Cu]^{2+}$ (including both one and two NO per Cu-dimer site, $[(NO)Cu\text{-}O\text{-}Cu]^{2+}$ and $[(NO)Cu\text{-}O\text{-}Cu(NO)]^{2+}$, respectively) as a result of the equilibrium shift of reactions (2-5) toward the right-hand sides at increasing concentrations of NO. These assignments are also consistent with DFT-predicted stable adsorbates involved in the low-temperature interactions and trends of vibrational frequencies, e.g., for 1T Cu-dimer models, $NO\text{-}[Cu\text{-}O\text{-}Cu]^{2+}$ (1871 cm^{-1}) ≈ $[(ON)Cu\text{-}O\text{-}Cu(NO)]^{2+}$ (1913 cm^{-1}), and $[(ON)Cu^{+}\cdots Cu^{+}(NO)]$ (1796 cm^{-1}) (Figure S14). Although different dimer configurations may result in small variations in the predicted vibrational frequencies, performing these calculations for all 115 unique positions in MFI is beyond the scope of this work; no significant changes are expected though.

Besides the two primary peaks, minor features are also present at 2156 and 1653 cm^{-1}, both of which exhibit monotonic increase in intensity with time. The peak at 2156 cm^{-1} can be assigned to NO^{+} associated with the Brønsted acid sites.[25] The 1653 cm^{-1} peak was not commonly observed in the previous spectroscopic studies of nitrogenous adsorbates on Cu-ZSM5. It could be associated with the $\nu_{as}(NO_2)$ stretching vibration in dinitrogen trioxide species (e.g., $Cu^{+}\text{-}O_2N{=}NO$,

with reported peak positions at 1644-1653 cm^{-1}),[71,72] which has previously been suggested as a critical intermediate for partial reduction of NO to N_2O on Cu monomers. However, this peak exhibits a clear downshift as the Si/Al ratio increases, reaching 1636 cm^{-1} for Cu-ZSM5-100 (Figure 4c), where the zeolite likely consists of isolated Cu cations (~ 80%, Fig. 2d).

Motivated by this observation, we used DFT calculations to study the reaction mechanism on isolated Cu cations in ZSM-5.[67,68,73] As summarized in Figure 3d, we concluded that the reaction mechanism proceeds through three transition states: TS1 (rotation of *NO to form *ON), TS2 (breaking of *ONNO to from bound *O and N_2O) and TS3 (reaction of bidente-NO_2 to form *NO_3). Our results show that adsorbed *NO_3 (denoted as ZCu-NO_3) represents the most stable state of isolated Cu monomers at low temperatures as the barriers for reactions with NO_2 (to form NO, 1.6 eV) and N_2O (to form NO, 2.4 eV) are likely insurmountable at 80 ºC. To further confirm the presence of ZCu-NO_3 for unpaired Al sites, we calculate the vibrational frequencies for all 12 unique T-sites using DFT. As summarized in Table S5 and also shown as insert in Figure 3d, the DFT predicted frequencies (1607 – 1650 cm^{-1}) are in very good agreement with experimental measurements (1636 cm^{-1}). Based on the above experimental observations and computational predictions, the interaction of Cu monomers with NO can be summarized as

$$Cu^{+} + 2NO + NO_2 \rightarrow Cu\text{-}NO_3 + N_2O \quad (6)$$

After assigning the spectroscopic features, we can now compare the spectra of the five types of Cu-ZSM5 with different Si/Al ratios. As also shown in Figure 4c, intensities of all the features reduce as the Si/Al ratio increases, as expected with the smaller Cu (or Al) site density in the zeolites. Interestingly the relative intensities of the two peaks at 1903 cm^{-1} and 1653-1636 cm^{-1} exhibit opposite trends. Specifically, the peak area ratio (1903 cm^{-1} versus 1653-1636 cm^{-1}) observed from DRIFTS scales well with $\eta_{Cu\cdots Cu}$ as derived from atomistic simulation and TPR

measurements, with a slope determined to be 6.66 (Figure 4e). As we discussed above, the two DRIFTS peaks are assigned to adsorbates associated with Cu dimers and monomers, which is also consistent with the relatively high stabilities of $[(NO)Cu\text{-}O\text{-}Cu]^{2+}$ (or $[(NO)Cu\text{-}O\text{-}Cu(NO)]^{2+}$) and $[Cu\text{-}NO_3]^{+}$ motifs associated with the corresponding Cu sites as suggested by DFT calculations (Figure 3a and S14). We have further compared the previously reported DRIFTS data[23,63,74] to our results in Figure 4e. As $\eta_{Cu\cdots Cu}$ was not resolved in these prior studies, we have estimated it by using the linear scaling relationship established in Figure 2d and the reported Cu-site densities. It can be seen that these data points also follow well the linear trend established for the Cu-ZSM5 catalysts in this work. The linear relationship shown in Figure 4e thus not only conforms the more favorable formation of Cu dimers at higher Cu site densities even under the reaction-relevant environment, but also indicates that the quantity $\eta_{Cu\cdots Cu}$ evaluated from CO/H_2-TPR measurements (with oxygen pretreatment, as shown in Figure 2d) is linearly correlated to the Cu-dimer fractions formed upon exposure to NO_x. It thus allows for employment of the established $\eta_{Cu\cdots Cu}$ to interpret the structures and properties of Cu-ZSM5 under reaction-relevant conditions.[35,75]

Titration of effluents. In addition to the spectroscopic analyses, we have performed independent measurements of the gaseous effluents during the low-temperature interaction of NO with Cu-ZSM5, to acquire more quantitative information of the adsorption properties. This was done under the same temperature and NO partial pressures, i.e., 80 ºC and 300 – 1500 ppm of NO, by using a plug flow reactor instead of the *in-situ* DRIFTS cell (see the Experimental Methods and Figure S15). The outlet gas is typically composed of N_2 and N_2O produced from the redox interactions between NO and the Cu sites in the zeolites, as well as residual nitric oxide (NO_{res}) left in the gas stream (Figures 5a, 5b and S16). The rate of NO adsorption (NO_{ad}) over the course was determined by calculating the mass balance of nitrogen (see the Supplementary Information

for the details). Quantitative summaries for the different molecule species are provided in Tables S6-S10. It should be pointed here that the differences in flow pattern, flow rate and catalyst loading between these two sets of experiments are not expected to alter the chemical nature and fractions of adsorbates at equilibrium (reached at the end of the adsorption process and determined by the concentration of NO and temperature), albeit variations in time scales to reach there.

The effluent profiles are featured with a long transient period before saturation, typically composed of three stages. Using 800 ppm NO on Cu-ZSM5-11.5 as an example, Figure 5a shows that during stage (I) (i.e. 0 – 384 min), only N_2 is present in the outlet. The concentration of produced N_2 initially rises with time and reaches the maximum of 268 ppm, and then drops from the peak value to 73 ppm. Correspondingly, the NO_{ad} profile presents a fast drop from nearly 800 ppm at the beginning to a minimum of 264 ppm, and then a rise to a peak value of 643 ppm. The amounts of NO_{res} and N_2O detected in the outlet are negligible in this stage. Stage (II) starts with a fast drop of NO_{ad} and rise of N_2O, both of which then reach a plateau at ~260 – 270 ppm and ~240 ppm, respectively. During this period, N_2 gradually phases out and no NO_{res} is present in the outlet. The last stage (III) is a transition process toward saturation, with both N_2O and NO_{ad} decreasing to zero and NO_{res} restoring to the feeding concentration (800 ppm). Similar behaviors are exhibited in the other adsorption profiles recorded on the different types of zeolites and/or at various concentrations of NO, albeit the variations in lengths and concentrations of nitrogenous species in each stage (Figures 5b and Figures S16).

The NO adsorption profiles presented above carry on abundant thermodynamic and kinetic information about the redox chemistry between NO and the Cu sites. Without going into the details of kinetics here, we focus on the cumulative production of N_2 and equilibrium state of NO_{ad} in the present discussion, aiming at assessing atomic structures and adsorption properties of the Cu sites

in the zeolites. As previously suggested in Figure S8, the production of N_2 from the low-temperature interaction between Cu-ZSM5 and NO can be attributed to the reaction[76]

$$[Cu^{+}\cdots Cu^{+}] + N_2O \rightarrow [Cu\text{-}O\text{-}Cu]^{2+} + N_2 \quad (7)$$

where N_2O can be derived from reaction (2) and (3). The total amount of N_2 detected during the NO adsorption process increases with P_{NO}, as more N_2O is accessible for reaction (7) (Figures 5c). A more interesting observation is the production of more N_2 for the zeolites with lower Si/Al ratios (Figures 5c). As indicated by the combination of reactions (3) and (7), the production of one N_2 molecule involves two Cu dimers. Cu monomers are associated with reaction (6) and would not contribute to the production of N_2 at the relatively low temperature (80 ^{o}C) employed here. Thereby the amount of N_2 produced from the NO adsorption process is also quantitatively indicative of the abundance of Cu dimers in the zeolites. The correlation between N_2 evolution and $\eta_{Cu\cdots Cu}$ exhibits a two-stage behavior (Figure S17). Fundamental understanding of these behaviors is obscured by the interweaving and competitive kinetics of reactions (6) and (7) during the interaction between Cu-ZSM5 and NO, but the more favorable production of N_2 at higher abundance of Cu dimers is obviously an outcome of the higher probability of an N_2O molecule generated from reaction (6) (or from Cu monomers in the process of forming $[Cu\text{-}NO_3]^{2+}$) to see another Cu dimer and get further reduced to N_2 via reaction (7). It is conceivable that this probability becomes less sensitive to the rise of $\eta_{Cu\cdots Cu}$ at high abundance of Cu sites, given with the expectation that it approaches saturation when $\eta_{Cu\cdots Cu}$ gets close to 1.

The specific capacity of NO adsorption is found to be insensitive to the Si/Al ratio, but to P_{NO} (Figure 5d). For example, the specific capacity is consistently at ~2.03 mmol/g_{Cu} for the five types of zeolites under 800 ppm of NO. Quantitative analysis of the NO adsorption capacities was performed in the framework of Ono-Kondo coordinates (see the Supplementary Information for

more details) to derive the adsorption energy (ΔE_{NO}) and "compression energy" (ΔE_{comp}).[77] The latter term (ΔE_{comp}) describes the interaction between adjacent adsorbates.[78,79] In the case of NO adsorption on Cu-ZSM5, ΔE_{comp} is indicative of the apparent difference in free energy between $[Cu\text{-}O\text{-}Cu(NO)]^{2+}$ and $[(NO)Cu\text{-}O\text{-}Cu(NO)]^{2+}$, namely the dimeric-Cu motifs with one or two NO adsorbates. Figure 5e shows the P_{NO}-dependent adsorption capacities plotted in the generalized Ono-Kondo coordinates for the five types of zeolites (at 80 ºC). ΔE_{NO} derived from the intercepts are determined to be ~33.5 kCal/mol for the Cu-ZSM5, which matches well with the calculated values of ~1.4 eV (32.2 kCal/mol) for $[Cu\text{-}O\text{-}Cu(NO)]^{2+}$. The negative slopes indicate positive ΔE_{comp}. The derived ΔE_{comp} is dependent on the Si/Al ratio and correspondingly $\eta_{Cu\cdots Cu}$, which varies from 2.55 kCal/mol for Cu-ZSM5-100 to 7.73 kCal/mol for Cu-ZSM5-11.5.

As ΔE_{comp} derived from the NO adsorption isotherms represents a statistic average of all Cu sites and no competitive adsorption of NO is expected on monomeric Cu sites (which are occupied by nitrate adsorbates, eq. (6)), we expect that the Cu-ZSM5 with more abundant Cu dimers will be more subjected to adsorption compression. This inference is confirmed with the positive and linear correlation between ΔE_{comp} and $\eta_{Cu\cdots Cu}$, as shown in Figure 5f. Noticeably, the calculated difference in free energy between $[(NO)Cu\text{-}O\text{-}Cu]^{2+}$ and $[(NO)Cu\text{-}O\text{-}Cu(NO)]^{2+}$ is about 0.3 eV, which corresponds well to the upbound value of ΔE_{comp} (~7-8 kCal/mol) observed from the Ono-Kondo analysis of the NO_{ad} capacities and confirms the compression energy measurement as a viable means to evaluate the adsorption properties of the Cu sites within Cu-ZSM5. Thereby ΔE_{comp} is a measurable descriptor of the adsorption properties for the Cu sites. Furthermore, a close view of their relationship finds slight deviation from the linear fitting, with ΔE_{comp} leveling off at high Cu dimer fractions. Such deviation indicates the presence of secondary effects, in addition to the population of dimers, contributing to the adsorption compression. It is

likely that the Cu···Cu distance[32,35,51,80] as well as the Cu-O-Cu bonding angle[26,36] have a weak dependence on the Si/Al ratio, probably originating from the Boltzmann (instead of completely random) distribution of Al sites that has led to somewhat more favorable exposure of certain Cu-dimer configurations (Table S2)[70,81,82] at low Si/Al ratios and high Cu site densities.

Bridge adsorption analytics and reaction kinetics. In the above discussion, we have established $\eta_{Cu\cdots Cu}$ and E_{comp} as quantitative descriptors for the atomic structures and adsorption properties of Cu-ZSM5 by combining atomistic simulation, TPR, DFT calculations and NO titration. Now we show that this analytic information can be used to interpret the catalytic performance of Cu-ZSM5 in NO decomposition reaction that takes place at elevated temperatures (>300 ^{o}C).

For all the five types of Cu-ZSM5, the measured NO conversion exhibits a nonlinear behavior in dependence of temperature, with the maximum reached at 400-450 ^{o}C (Figure 6a). The drop of NO conversion at temperatures above 450 ^{o}C is not a result of equilibrium shift (Figure S18), neither due to catalyst deactivation (Figure S19). Throughout the temperature range (350-550 ^{o}C) investigated here, the NO conversion decreases as Si/Al ratio increases. At 450 ^{o}C, the NO conversion varies from 85.2% on Cu-ZSM5-11.5 to 46.6% on Cu-ZSM5-30, and to only 2.6% on Cu-ZSM5-100. Both N_2 and N_2O were detected as product, and the selectivity toward N_2 increases with temperatures (Figure S20). The formation of N_2 during NO decomposition can be via reactions (7) and

$$[Cu\text{-}O\text{-}Cu]^{2+} + N_2O \rightarrow [Cu\text{-}O_2\text{-}Cu]^{2+} + N_2 \quad (8)$$

$$[Cu\text{-}O_2\text{-}Cu]^{2+} \rightarrow [Cu^{+}\cdots Cu^{+}] + O_2 \quad (9)$$

where reactions (8) and (9)[34,35] are required for regeneration of the dimeric Cu sites (see Figure 3a for the scheme). Among the different catalysts, the zeolites with lower Si/Al ratios have higher N_2

selectivity, with Cu-ZSM5-11.5 achieving 99% at 450 ºC. It is further found that the zeolite with higher Cu dimer fraction gives higher specific rates (per Cu site) of N_2 formation (Figure 6b). It can be concluded from these findings that the Cu dimers are active sites for the decomposition of NO to N_2. This conclusion is further supported by the comparison of calculated NO decomposition pathways for the two types of Cu sites (Figure 3), which shows that the pathway toward N_2 on monomers via reactions (6) and

$$[\text{Cu-NO}_3]^+ \rightarrow [\text{Cu-NO}]^+ + \text{O}_2 \quad (10)$$

is much less favorable primarily due to the much higher reaction energy of (10) than (9). Noticeably, the N_2 selectivity correlates well to the measured N_2 evolution from the low-temperature titration experiments (Figure 6c), expectable as the abundance of Cu dimers governs the pathway toward N_2 in both cases.

Kinetic measurements were further performed on the Cu-ZSM5 catalysts at reduced loadings. The derived apparent rate constant (k_{app}) for N_2 formation exhibits a two-stage linear behavior in the Arrhenius plots (Figure 6d). In the low-temperature region (e.g., $T < 400$ ºC for Si/Al = 11.5, 20 and 30), k_{app} increases with temperature, indicating a positive activation energy ($E_{app,1} > 0$), whereas an opposite scenery for negative activation energy ($E_{app,2} < 0$) is discerned in the high-temperature region. The maximal k_{app} is also reached at ~400-450 ºC, suggesting that the volcano shape in the dependence of NO conversion on temperature (Figure 6a) is a result of kinetic effects.[15,76,83] Similar to the observation in NO conversion, the Cu-ZSM5 with lower Si/Al ratios have larger k_{app}, in line with the previous reports on Cu-ZSM5 of the same Si/Al ratio but different Cu exchange levels.[37,84] According to the kinetic model reported by Modén *et al*. (see the Supplementary Information for more details),[15] the two-stage behavior of Cu-ZSM5 is due to the interplay of NO decomposition (as shown in Figure 2a) and oxygen evolution pathways, with the

latter likely limiting the reaction rate at relatively low temperatures (e.g., <400 ºC) but becoming feasible at more elevated temperatures. The impact of Cu atomic structures on the reaction kinetics is better visualized by plotting ln(k_{app}) versus $\eta_{Cu\cdots Cu}$ (Figure 6e). The nearly linear relationships at both low and high temperatures underlines the above conclusion with Cu dimers being the active sites for decomposition of NO to N_2. The different slopes, *i.e.*, 7.0 @ 350 ºC versus 3.7 @ 550 ºC, are indicative of the dissimilar weighing factors of the structure effects on the reaction kinetics, as the low-temperature reaction rate is limited by both NO conversion and oxygen evolution, both of which are more favorable on Cu dimers, whereas the high-temperature rate is only governed by NO conversion that becomes feasible on both dimers and monomers in this condition (e.g., at >400 ºC). We further found that both $E_{app,1}$ and $E_{app,2}$ correlate well to the adsorption property, ΔE_{comp}, derived from the NO titration measurements (Figure 5f). The direct correlations of these energetic functions are indicative of and the experimental measure of the underlying scaling relationships among the free energies of various adsorbates and transition states involved in the NO decomposition reaction in dependence of the Cu-motif atomic structures, namely more Cu dimers giving rise to more compression in the NO adsorption isotherm, reduced energy barriers for NO conversion and more favorable oxygen evolution (as compared to Cu monomers). Moreover, the better linear fitting for the correlation between E_{app} and ΔE_{comp} than with $\eta_{Cu\cdots Cu}$ (Figure S21) suggest that the secondary structural effects (e.g., Cu···Cu distance[32,35,78,79] and Cu-O-Cu bonding angle[26,36]), as captured by the adsorption compression energy measurements, also propagate to the catalytic reaction kinetics. The successful use of $\eta_{Cu\cdots Cu}$ and E_{comp} to interpret the catalytic performance of Cu-ZSM5 thus bridged the low-temperature adsorption analytics and the high-temperature reaction kinetics.

General applicability of $\eta_{Cu\cdots Cu}$ and E_{comp} as descriptors. As discussed above, it is clear that $\eta_{Cu\cdots Cu}$ and E_{comp} are valuable descriptors for both the structure and reactivity of Cu-ZSM5. In the following we further show that the established relationships can be generalized to other types of zeolites and reactions.

Similar to Cu-ZSM-5, copper-exchanged MOR and SSZ-13 are also important industrial catalysts that contain Cu-dimer active sites.[51,85-87] We have synthesized Cu-MOR-10 and Cu-SSZ13-11, both at full exchange (Cu/Al ~ 0.5), for which $\eta_{Cu\cdots Cu}$ is measured to be ca. 43% and 28%, respectively (Figure S22 and Table S11), in consistent with literature results with similar Cu densities (Figure S23).[88-90] DRIFTS analysis and chemical titration of the reactive adsorption of NO on these two types of copper-exchanged zeolites (Figure S24-S27 and Table S12-S14) confirm that they also follow the established linear relationships correlating the spectroscopic features (Figure 4e and Figure S28a), NO-adsorption compression energy (Figure 5f and Figure S28b) and the Cu-dimer fraction. Moreover, catalytic studies for NO decomposition indicates that $\eta_{Cu\cdots Cu}$ and E_{comp} quantified for Cu-MOR and Cu-SSZ13 can also describe their reaction kinetics (Figure S29 and S30). The general applicability of these correlations for copper-exchanged zeolites confirms the established bridges between adsorption analytics and catalytic kinetics and is also in line with the expectation that they are characteristic of the Cu-dimer motifs forming on aluminosilicate substrates.

In addition to NO decomposition, we have applied $\eta_{Cu\cdots Cu}$ and E_{comp} as descriptors to interpret the kinetics of methane-to-methanol (MTM) conversion. Cu-ZSM5 has been extensively studied for the MTM reaction.[19,26,53,85,90,91] Although $[CuOCu]^{2+}$ has been identified as the active sites for methane activation,[42] quantitative correlation of the Cu-dimer fraction (or number density) to the catalytic activity is few reported for MTM. Based on the average copper site densities recorded in

the literature studies,[19,26,91-93] we have estimated the corresponding copper dimer fractions and compression energies using the linear relationships established in Figures 2d and 5f (see Table S15 and Figure S31). The estimated copper dimer fractions were confirmed by comparing them to the values determined in this study (Figure S32). Linear relationships are thus established between the MTM reactivity and $\eta_{Cu\cdots Cu}$ (Figure 7a), as well as between the activation energy and E_{comp} (Figure 7b). To validate the robustness and predictive capability of these relationships, we have further performed our own measurements of MTM on Cu-ZSM5-11.5 and Cu-ZSM5-20 (see the experimental methods in the Supplementary Information). These two catalysts produced 18.4 and 13.0 μmol of methanol per gram of catalyst at 200 ^{o}C, respectively (Figure S33). The corresponding activation energies are determined to be 77.7 and 80.0 kJ/mol (Figure S34). Such values are in line with the previous reports with similar copper site densities (Figure S35).[91,92] As shown in Figure 7, the measured catalytic performance falls onto the as-established linear relationships. It thus confirms the general applicability of $\eta_{Cu\cdots Cu}$ and E_{comp} as quantitative descriptors for the MTM reaction.

CONCLUSION

We have combined atomistic simulation, chemisorption and titration measurements to obtain reaction-relevant structural and property information of Cu exchanged ZSM5. The established descriptors such as $\eta_{Cu\cdots Cu}$ and ΔE_{comp} are validated to be applicable to Cu-ZSM5 prepared in this study and also other data reported in the literature. They are found to correlate well to the catalytic performance of the Cu-ZSM5 catalysts for NO decomposition. Our studies have established multiple linear correlations between the adsorption analytics and reaction kinetic parameters, which reflect the intrinsic scaling relationships governing the adsorption and catalytic properties

of the metal sites within the zeolite. These relationships have further been generalized to understand the structure-property relationships of other metal-exchanged zeolites and interpretation of the catalytic performance of Cu-ZSM5 for the methane-to-methanol conversion. The quantitative descriptors and the corresponding correlations are thus believed to be valid for guiding the design and development of advanced catalytic materials for various reactions.

ACKNOWLDEGEMENTS

This work was supported by the Department of Energy, Advanced Research Projects Agency-Energy (ARPA-E). PX and CW also acknowledge the support by the Petroleum Research Fund, American Chemical Society. AK acknowledges the use of computing resources provided by the National Energy Research Scientific Computing Center (NERSC), a U.S. Department of Energy Office of Science User Facility operated under Contract No. DE-AC02-05CH11231 and the Extreme Science and Engineering Discovery Environment (XSEDE), which is supported by National Science Foundation grant number ACI-1548562.

Table 1. Bulk elemental analysis and BET Surface Area for Cu-Zeolites with different Si/Al ratios.

Si/Al	Cu/Al	Surface Area ($m^2\ g^{-1}$)	Cu Loading (μmol/g)	Cu Site Density ($\times 1000\ Å^{-3}$)	Average Cu···Cu Distance (Å)
11.5	0.51	373	487.80	0.52	15.4
20	0.51	373	336.74	0.36	17.4
30	0.48	406	292.68	0.31	18.2
50	0.49	385	154.21	0.17	22.6
100	0.47	396	74.59	0.08	28.8

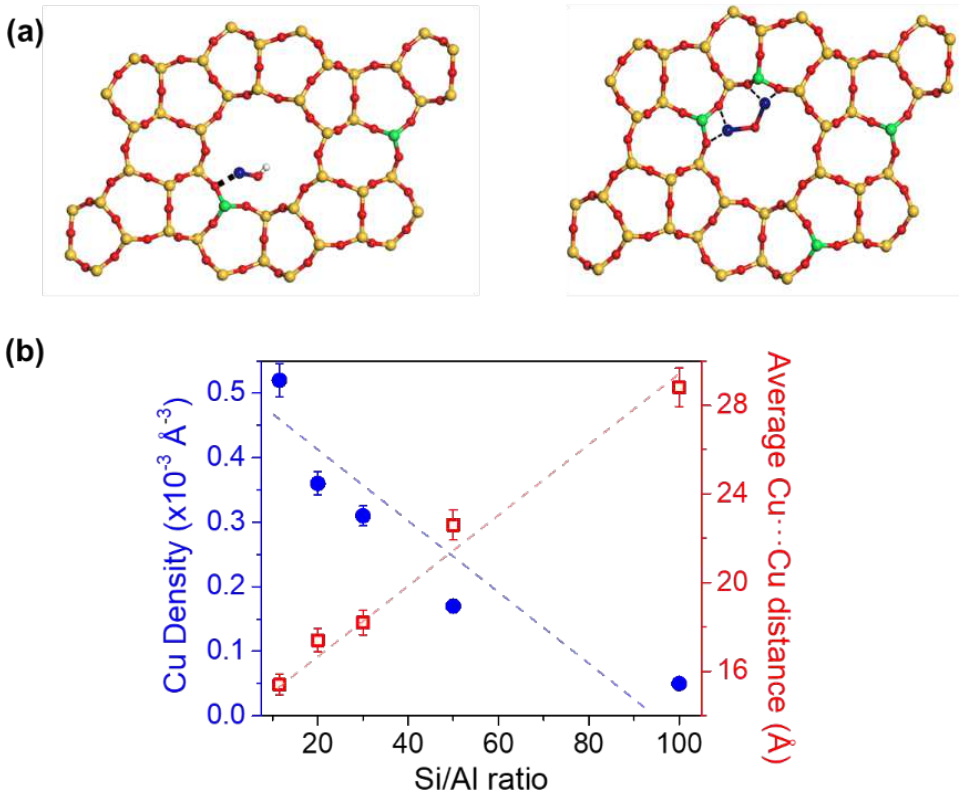

Figure 1. Graphical illustration and characterization of Cu sites in ZSM5. (a) Geometric models of a Cu monomer site (left) and an oxygen bridged Cu dimer site (right) in Cu-ZSM5. (b) Dependence of Cu density (per unit volume of the zeolite pore) and average Cu-Cu distance on Si/Al ratio in Cu-ZSM5.

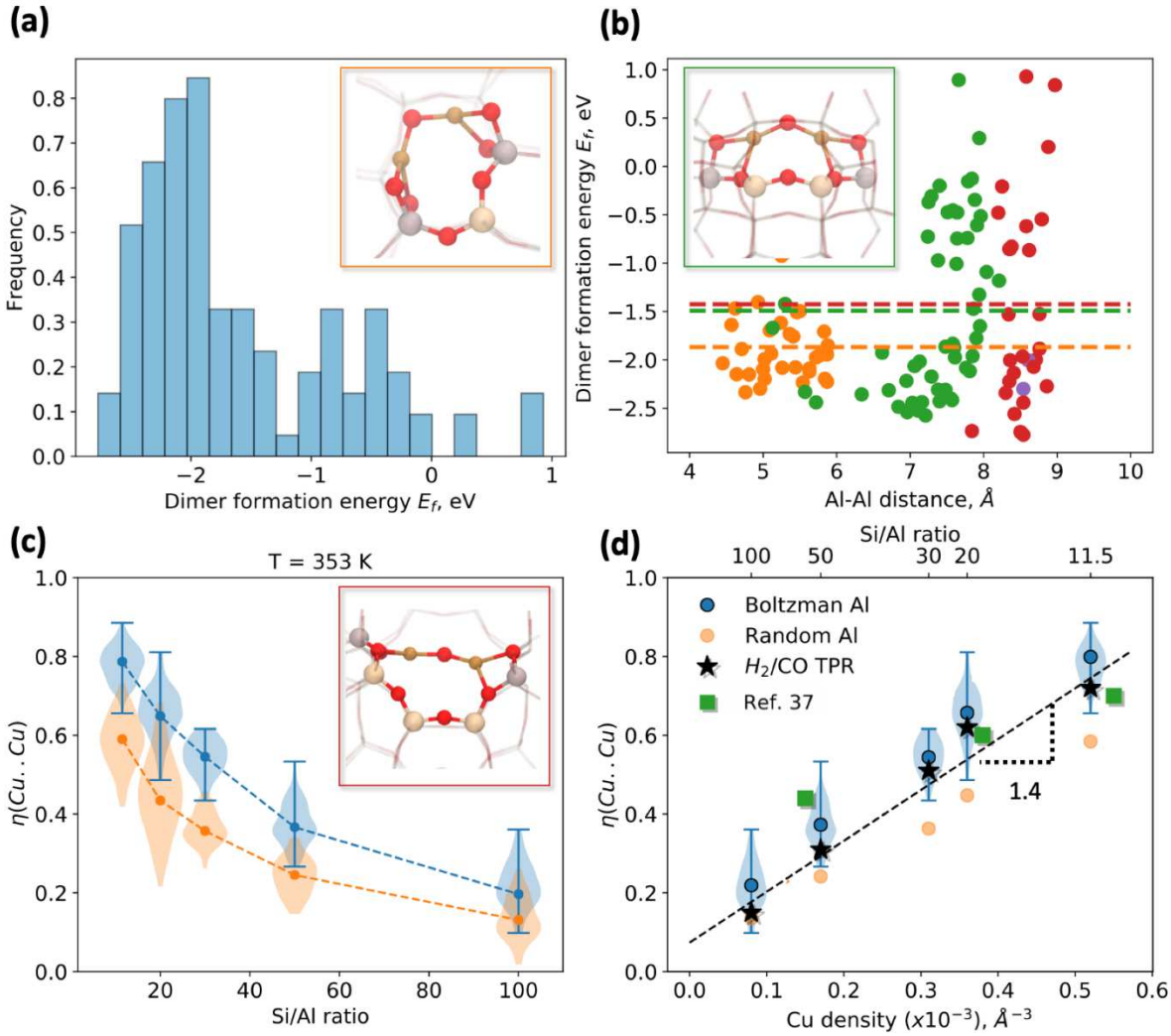

Figure 2. (a) Histogram showing the distribution of dimer formation energies (E_f) for all possible $[CuOCu]^{2+}$ dimers in MFI. (b) E_f at different Al-Al distances and #Si atoms between the 2Al atoms: 1T (orange), 2T (green), 3T (red) and 4T (purple); the dotted lines show the average E_f. (c) Fraction of Cu dimers in MFI, η(Cu..Cu) at 80 °C assuming a Boltzmann-weighted (blue) and random (orange) distribution of Al atoms. (d) Linear relationship between the Cu dimer fraction derived from DFT calculations (blue) and TPR measurements (black stars) with Cu density and Si/Al ratio. The experimental data from Ref. 37 (green squares) is consistent with our computational predictions. The insets in (a), (b) and (c) show the structures of the most favorable 1T, 2T and 3T dimer configuration in MFI.

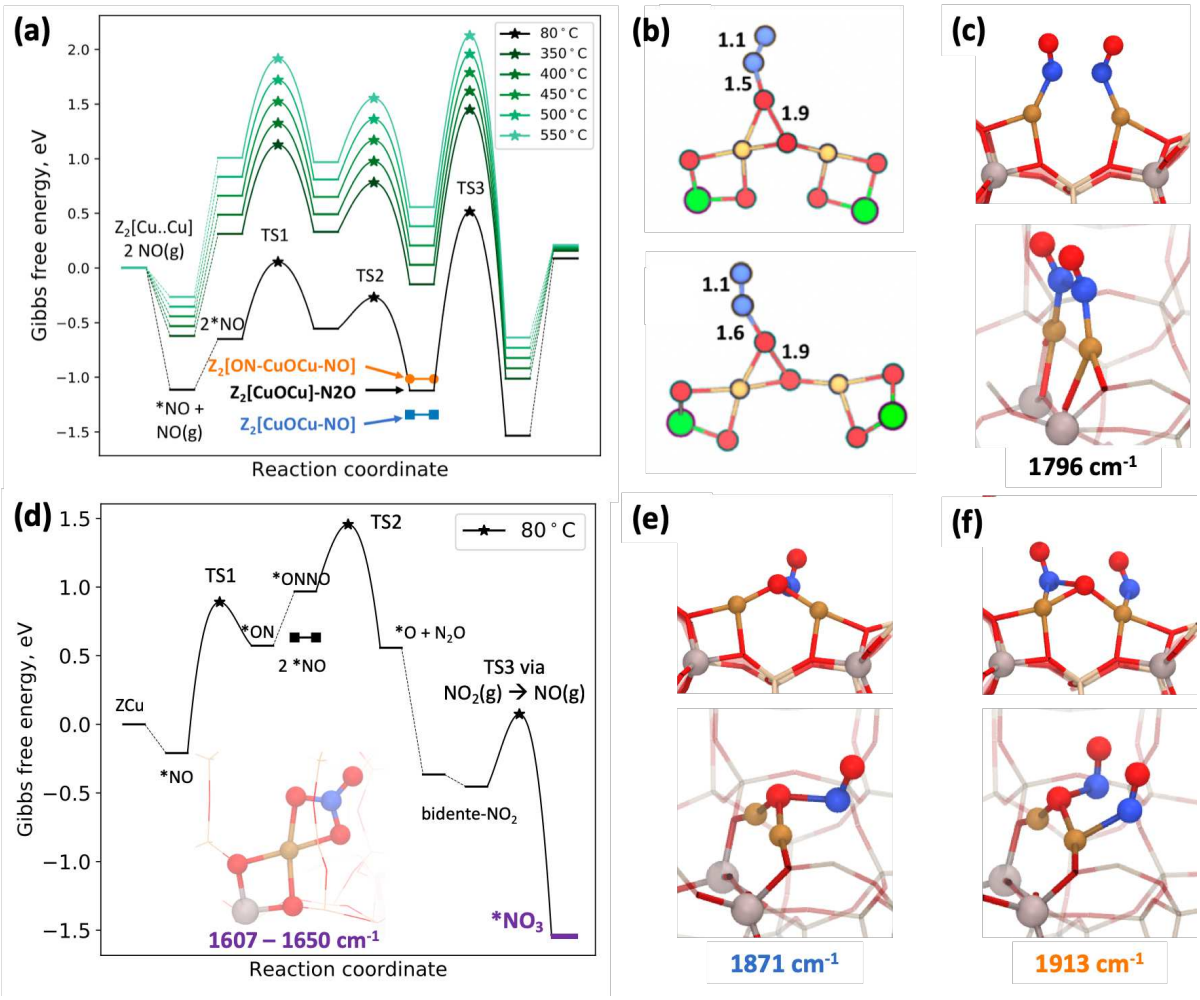

Figure 3. (a) DFT calculated free energy diagrams at various temperatures for NO decomposition by Cu dimers in 1T-MFI; free energies of one and two NO bound dimers are shown in orange and blue, respectively. (b) The transition states for N_2O decomposition for 1T (upper) and 2T (lower) models (Red: O, Blue: N, Yellow: Cu, Green: Al), (c) – (f) structure model and vibrational frequencies for $[(ON)Cu^{+}\cdots Cu^{+}(NO)]$, $[Cu\text{-}NO_3]^{+}$, $NO\text{-}[Cu\text{-}O\text{-}Cu]^{2+}$ and $[(NO)Cu\text{-}O\text{-}Cu(NO)]^{2+}$, respectively (Red: O, Blue: N, Yellow: Cu, Gray: Al). The free energy diagram for the isolated-Cu site is shown in (d) at 80 °C.

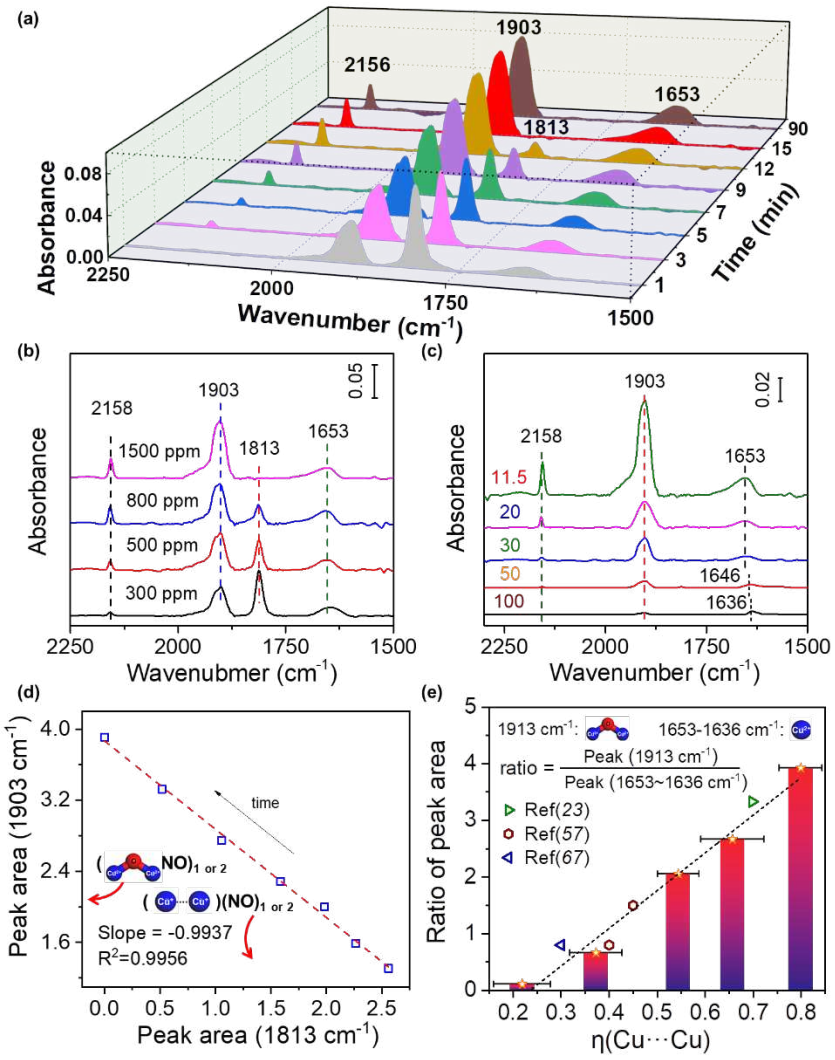

Figure 4. Characterization and quantification of Cu dimers in Cu-ZSM5 zeolites. (a) Time dependence DRIFTs of NO isothermal adsorption at 80 ºC on Cu-ZSM5-11.5 at 1500 ppm. (b) Pressure dependence DRIFTs of NO isothermal adsorption at 80 ºC on Cu-ZSM5-11.5 at 15 min. (c) DRIFTs of NO isothermal adsorption at 80 ºC on Cu-ZSM5 with different Si/Al ratios at 1500 ppm and 15 min. (d) Correlation of integrated peak areas of 1903 cm^{-1} peak and 1813 cm^{-1} peak in DRIFT spectra of NO isothermal adsorption at 80 ºC and 1500 ppm on Cu-ZSM5-11.5 at different times. (e) Correlation of area ratios of 1903 cm^{-1} peak and 1813 cm^{-1} peak in DRIFT spectra of NO isothermal adsorption at 80 ºC on Cu-ZSM5 and Cu dimer fraction from DFT calculation and TPR measurements.

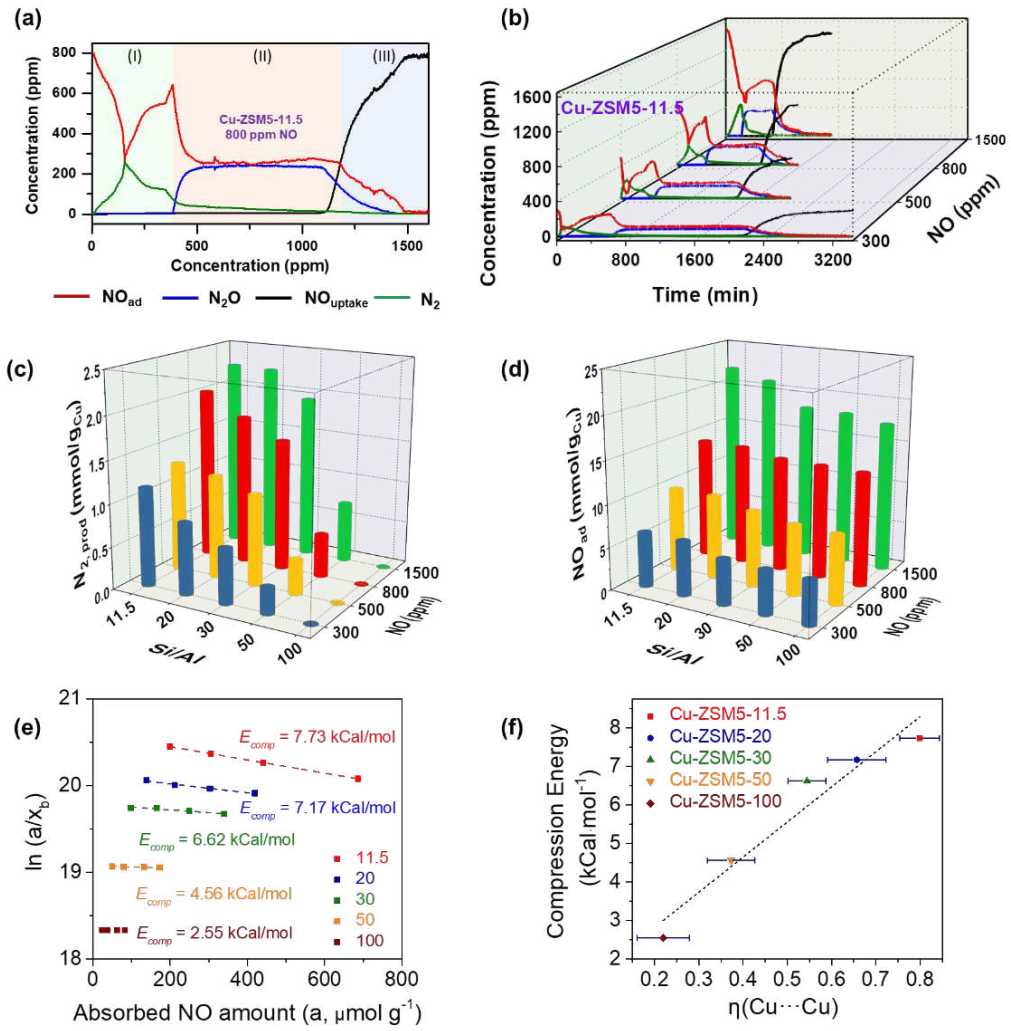

Figure 5. NO Isothermal adsorption profiles. (NO_{ad}: red, $N_{2,prod}$: green, N_2O_{prod}: blue, NO_{uptake}: black) (a) Time dependent profiles of outlet concentrations of NO, N_2O and N_2 during NO isothermal adsorptions at 80 ºC with 800 ppm of NO on Cu-ZSM5-11.5. (b) Time dependent plot of outlet concentrations of NO, N_2O and N_2 during NO isothermal adsorptions at 80 ºC with different pressures of NO for Cu-ZSM5-11.5. (c) plot of N_2 production per Cu site during NO isothermal adsorption at different NO pressures on the five Cu-ZSM5. (d) plots of adsorbed NO per Cu site during NO isothermal adsorption at different NO pressures on Cu-ZSM5 zeolites. (e) Ono-Kondo plots for compression energies of Cu-ZSM5 zeolites. (f) Correlation of calculated compression energy and average Cu-Cu distance in Cu-ZSM5 zeolites.

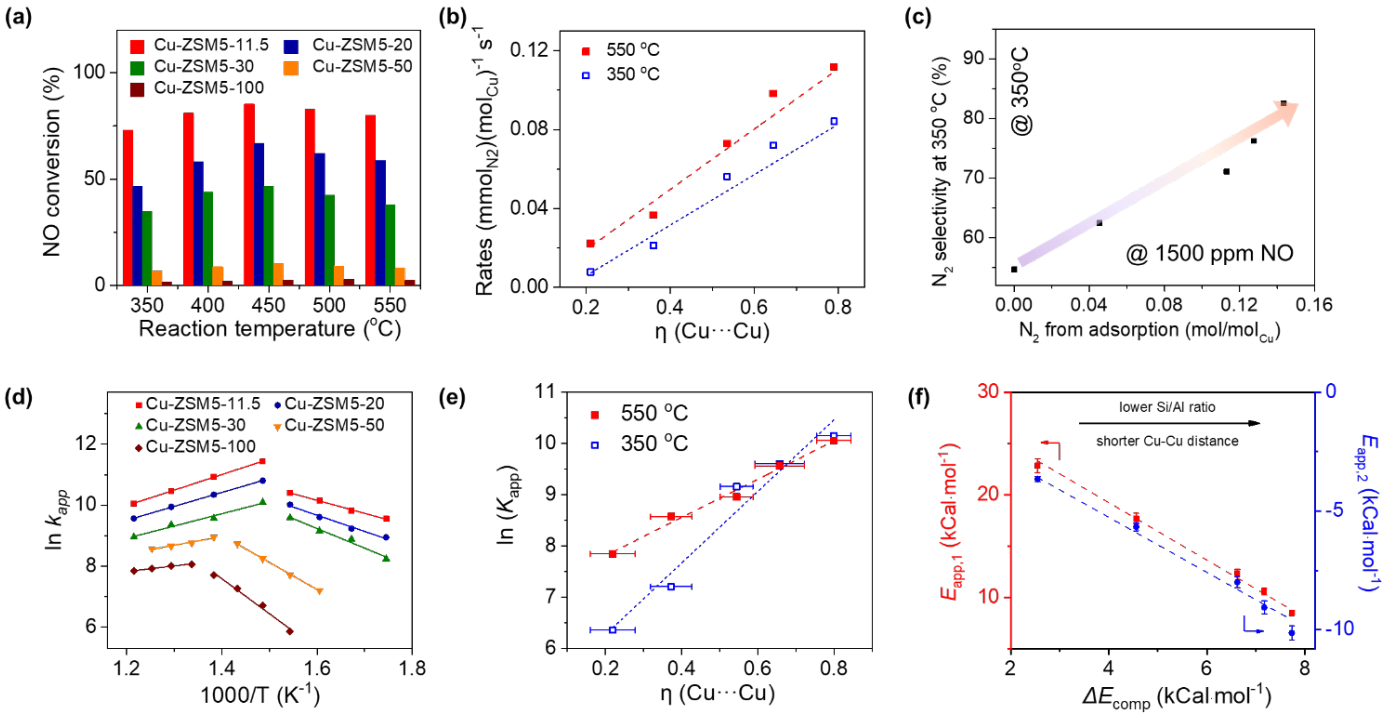

Figure 6. Catalytic performance and Kinetics of NO Decomposition. (a) Conversions of NO over different Cu-ZSM5. (b) Correlations between rates of N_2 at 350, 550 °C and fractions of Cu dimers. (c) Trends of N_2 selectivity at 350 depending on N_2 production during NO isothermal adsorptions at 80 °C with 1500 ppm of NO on Cu-ZSM5 zeolites. (d) Arrhenius plots for rate constants vs 1/T. (e) Correlations between ln(K_{app}) at 350, 550 °C and fractions of Cu dimers fractions. (f) Correlation of apparent activation energies at low temperatures (red, left) and at high temperatures (blue, right) with compression energy derived from Ono-Kondo coordinates.

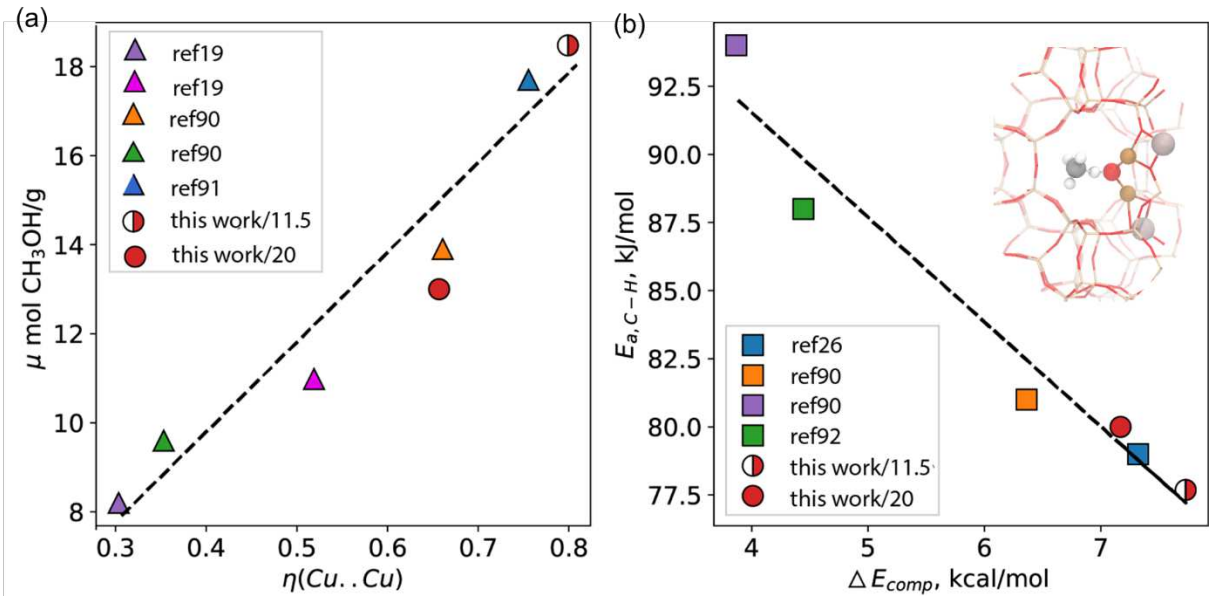

Figure 7. Catalytic study of methane to methanol by using Cu-ZSM5 from the literature and this work. (a) Correlations between the methanol yields with Cu dimers fractions; (b) Correlation of apparent methane activation energies with compression energies. Hereby the Cu dimers fractions and compression energies are derived by fitting the Cu densities from literature into the scaling established in Figure 2d and Figure 5f.

References

1 Weckhuysen, B. M. Snapshots of a working catalyst: possibilities and limitations of in situ spectroscopy in the field of heterogeneous catalysis. *Chem. Commun.*, 97-110, (2002).

2 Yang, J. C., Small, M. W., Grieshaber, R. V. & Nuzzo, R. G. Recent developments and applications of electron microscopy to heterogeneous catalysis. *Chem. Soc. Rev.* **41**, 8179-8194, (2012).

3 Bordiga, S., Groppo, E., Agostini, G., van Bokhoven, J. A. & Lamberti, C. Reactivity of Surface Species in Heterogeneous Catalysts Probed by In Situ X-ray Absorption Techniques. *Chem. Rev.* **113**, 1736-1850, (2013).

4 Zaera, F. New advances in the use of infrared absorption spectroscopy for the characterization of heterogeneous catalytic reactions. *Chem. Soc. Rev.* **43**, 7624-7663, (2014).

5 Wachs, I. E. & Roberts, C. A. Monitoring surface metal oxide catalytic active sites with Raman spectroscopy. *Chem. Soc. Rev.* **39**, 5002-5017, (2010).

6 Andersson, M. P., Bligaard, T., Kustov, A., Larsen, K. E., Greeley, J., Johannessen, T., Christensen, C. H. & Norskov, J. K. Toward computational screening in heterogeneous catalysis: Pareto-optimal methanation catalysts. *J. Catal.* **239**, 501-506, (2006).

7 Norskov, J. K., Bligaard, T., Rossmeisl, J. & Christensen, C. H. Towards the computational design of solid catalysts. *Nat. Chem.* **1**, 37-46, (2009).

8 Haneda, M. & Hamada, H. Recent progress in catalytic NO decomposition. *CR Chim.* **19**, 1254-1265, (2016).

9 Zhang, R. D., Liu, N., Lei, Z. G. & Chen, B. H. Selective Transformation of Various Nitrogen-Containing Exhaust Gases toward N_2 over Zeolite Catalysts. *Chem. Rev.* **116**, 3658-3721, (2016).

10 Li, Y. J. & Hall, W. K. Catalytic Decomposition of Nitric-Oxide over Cu-Zeolites. *J. Catal.* **129**, 202-215, (1991).

11 Grunert, W. H., N. W. Joyner, R. W. Shpiro, E. S. Siddiqui, M. R. H. & Baeva, G. N. Structure, Chemistry, and Activity of Cu-Zsm-5 Catalysts for the Selective Reduction of Nox in the Presence of Oxygen. *J. Phy. Chem.* **98**, 10832-10846, (1994).

12 Trout, B. L., Chakraborty, A. K. & Bell, A. T. Analysis of the thermochemistry of NOx decomposition over CuZSM-5 based on quantum chemical and statistical mechanical calculations. *J. Phy. Chem.* **100**, 17582-17592, (1996).

13 Lamberti, C. B., S. Salvalaggio, M. Spoto, G. Zecchina, A. Geobaldo, F. Vlaic, G. & Bellatreccia, M. XAFS, IR, and UV-vis study of the Cu^{I} environment in Cu^{I}-ZSM-5. *J. Phys. Chem. B* **101**, 344-360, (1997).

14 Schneider, W. F., Hass, K. C., Ramprasad, R. & Adams, J. B. Density functional theory study of transformations of nitrogen oxides catalyzed by Cu-exchanged zeolites. *J. Phys. Chem. B* **102**, 3692-3705, (1998).

15 Moden, B., Da Costa, P., Fonfe, B., Lee, D. K. & Iglesia, E. Kinetics and mechanism of steady-state catalytic NO decomposition reactions on Cu-ZSM5. *J. Catal.* **209**, 75-86, (2002).

16 Kuroda, Y. & Iwamoto, M. Characterization of cuprous ion in high silica zeolites and reaction mechanisms of catalytic NO decomposition and specific N_2 adsorption. *Top. Catal.* **28**, 111-118, (2004).

17 Snyder, B. E. R., Bols, M. L., Schoonheydt, R. A., Sels, B. F. & Solomon, E. I. Iron and Copper Active Sites in Zeolites and Their Correlation to Metalloenzymes. *Chem. Rev.* **118**, 2718-2768, (2018).

18 Groothaert, M. H., Lievens, K., Leeman, H., Weckhuysen, B. M. & Schoonheydt, R. A. An operando optical fiber UV-vis spectroscopic study of the catalytic decomposition of NO and N_2O over Cu-ZSM-5. *J. Catal.* **220**, 500-512, (2003).

19 Groothaert, M. H., Smeets, P. J., Sels, B. F., Jacobs, P. A. & Schoonheydt, R. A. Selective oxidation of methane by the bis(mu-oxo)dicopper core stabilized on ZSM-5 and mordenite zeolites. *J. Am. Chem. Soc.* **127**, 1394-1395, (2005).

20 Giordanino, F. V., P. N. R. Lundegaard, L. F. Stappen, F. N. Mossin, S. Beato, P. Bordiga, S. & Lamberti, C. Characterization of Cu-exchanged SSZ-13: a comparative FTIR, UV-Vis, and EPR study with Cu-ZSM-5 and Cu-beta with similar Si/Al and Cu/Al ratios. *Dalton. T.* **42**, 12741-12761, (2013).

21 Palomino, G. T. F., P. Bordiga, S. Zecchina, A. Giamello, E. & Lamberti, C. Oxidation states of copper ions in ZSM-5 zeolites: A multitechnique investigation. *J. Phys. Chem. B* **104**, 4064-4073, (2000).

22 Beutel, T., Sarkany, J., Lei, G. D., Yan, J. Y. & Sachtler, W. M. H. Redox chemistry of Cu/ZSM-5. *J. Phys. Chem.* **100**, 845-851, (1996).

23 Konduru, M. V. & Chuang, S. S. C. Investigation of adsorbate reactivity during NO decomposition over different levels of copper ion-exchanged ZSM-5 using in situ IR technique. *J. Phys. Chem. B* **103**, 5802-5813, (1999).

24 Tortorelli, M., Chakarova, K., Lisi, L. & Hadjiivanov, K. Disproportionation of associated Cu^{2+} sites in Cu-ZSM-5 to Cu^{+} and Cu^{3+} and FTIR detection of $Cu^{3+}(NO)_x$ (x=1, 2) species. *J. Catal.* **309**, 376-385, (2014).

25 Fanson, P. T., Stradt, M. W., Lauterbach, J. & Delgass, W. N. The effect of Si/Al ratio and copper exchange level on isothermal kinetic rate oscillations for N_2O decomposition over Cu-ZSM-5: a transient FTIR study. *Appl. Catal. B* **38**, 331-347, (2002).

26 Woertink, J. S., Smeets, P. J., Groothaert, M. H., Vance, M. A., Sels, B. F., Schoonheydt, R. A. & Solomon, E. I. A $[Cu_2O]^{2+}$ core in Cu-ZSM-5, the active site in the oxidation of methane to methanol. *PNAS* **106**, 18908-18913, (2009).

27 Smeets, P. J. H., R. G. Woertink, J. S. Vanelderen, P. Schoonheydt, R. A. Sels, B. F. & Solomon, E. I. Oxygen Precursor to the Reactive Intermediate in Methanol Synthesis by Cu-ZSM-5. *J. Am. Chem. Soc.* **132**, 14736-14738, (2010).

28 Larsen, S. C., Aylor, A., Bell, A. T. & Reimer, J. A. Electron-Paramagnetic-Resonance Studies of Copper Ion-Exchanged ZSM-5. *J. Phys. Chem.* **98**, 11533-11540, (1994).

29 Soria, J., Martinez-Arias, A., Martinez-Chaparro, A., Conesa, J. C. & Schay, Z. Influence of the preparation method, outgassing treatment, and adsorption of NO and/or O_2 on the Cu^{2+} species in Cu-ZSM-5: An EPR study. *J. Catal.* **190**, 352-363, (2000).

30 Groothaert, M. H., Pierloot, K., Delabie, A. & Schoonheydt, R. A. Identification of Cu(II) coordination structures in Cu-ZSM-5, based on a DFT/ab initio assignment of the EPR spectra. *Phys. Chem. Chem. Phys.* **5**, 2135-2144, (2003).

31 Neylon, M. K., Marshall, C. L. & Kropf, A. J. In situ EXAFS analysis of the temperature-programmed reduction of Cu-ZSM-5. *J. Am. Chem. Soc.* **124**, 5457-5465, (2002).

32 Groothaert, M. H., van Bokhoven, J. A., Battiston, A. A., Weckhuysen, B. M. & Schoonheydt, R. A. Bis(μ-oxo)dicopper in Cu-ZSM-5 and its role in the decomposition of NO: A combined in situ XAFS, UV-Vis-Near-IR, and kinetic study. *J. Am. Chem. Soc.* **125**, 7629-7640, (2003).

33 Shido, T. Y., A. Inada, Y. Asakura, K. Nomura, M. & Iwasawa, Y. Dispersive XAFS study on Cu and Mo species in zeolites during the catalyst preparation. *Top. Catal.* **18**, 53-58, (2002).

34 Sajith, P. K., Shiota, Y. & Yoshizawa, K. Role of Acidic Proton in the Decomposition of NO over Dimeric Cu(I) Active Sites in Cu-ZSM-5 Catalyst: A QM/MM Study. *ACS Catal.* **4**, 2075-2085, (2014).

35 Moretti, G. F., G. Fierro, G. Lo Jacono, M. Morpurgo, S. & Faticanti, M. Dimeric Cu(I) species in Cu-ZSM-5 catalysts: the active sites for the NO decomposition. *J. Catal.* **232**, 476-487, (2005).

36 Tsai, M. L. H., R. G. Vanelderen, P. Sels, B. F. Schoonheydt, R. A. & Solomon, E. I. $[Cu_2O]^{2+}$ Active Site Formation in Cu-ZSM-5: Geometric and Electronic Structure Requirements for N_2O Activation. *J. Am. Chem. Soc.* **136**, 3522-3529, (2014).

37 Da Costa, P. M., B. Meitzner, G. D. Lee, D. K. Iglesia, E. Spectroscopic and chemical characterization of active and inactive Cu species in NO decomposition catalysts based on Cu-ZSM5. *Phys. Chem. Chem. Phys.* **4**, 4590-4601, (2002).
38 Armor, J. N. Metal-exchanged zeolites as catalysts. *Micropor. Mesopor. Mat.* **22**, 451-456, (1998).
39 Brandenberger, S., Krocher, O., Tissler, A. & Althoff, R. The State of the Art in Selective Catalytic Reduction of NO_x by Ammonia Using Metal-Exchanged Zeolite Catalysts. *Catal. Rev.* **50**, 492-531, (2008).
40 Yang, S. T., Kim, J. & Ahn, W. S. CO_2 adsorption over ion-exchanged zeolite beta with alkali and alkaline earth metal ions. *Micropor. Mesopor. Mat.* **135**, 90-94, (2010).
41 Hudson, M. R. Q., W. L. Mason, J. A. Fickel, D. W. Lobo, R. F. & Brown, C. M. Unconventional, Highly Selective CO_2 Adsorption in Zeolite SSZ-13. *J. Am. Chem. Soc.* **134**, 1970-1973, (2012).
42 Ravi, M. S., V. L. Knorpp, A. J. Newton, M. A. Palagin, D. Pinar, A. B. Ranocchiari, M. van Bokhoven, J. A. Misconceptions and challenges in methane-to-methanol over transition-metal-exchanged zeolites. *Nat. Catal.* **2**, 485-494, (2019).
43 Di Iorio, J. R. & Gounder, R. Controlling the Isolation and Pairing of Aluminum in Chabazite Zeolites Using Mixtures of Organic and Inorganic Structure-Directing Agents. *Chem. Mater.* **28**, 2236-2247, (2016).
44 Kustova, M. Y., Rasmussen, S. B., Kustov, A. L. & Christensen, C. H. Direct NO decomposition over conventional and mesoporous Cu-ZSM-5 and Cu-ZSM-11 catalysts: Improved performance with hierarchical zeolites. *Appl. Catal. B* **67**, 60-67, (2006).
45 Xie, P. F., Ma, Z., Zhou, H. B., Huang, C. Y., Yue, Y. H., Shen, W., Xu, H. L., Hua, W. M. & Gao, Z. Catalytic decomposition of N_2O over Cu-ZSM-11 catalysts. *Micropor. Mesopor. Mat.* **191**, 112-117, (2014).
46 Xie, P. F., Luo, Y. J., Ma, Z., Wang, L. Y., Huang, C. Y., Yue, Y. H., Hua, W. M. & Gao, Z. CoZSM-11 catalysts for N2O decomposition: Effect of preparation methods and nature of active sites. *Appl. Catal. B* **170**, 34-42, (2015).
47 Gao, F., Kollar, M., Kukkadapu, R. K., Washton, N. M., Wang, Y. L., Szanyi, J. & Peden, C. H. F. Fe/SSZ-13 as an NH3-SCR catalyst: A reaction kinetics and FTIR/Mossbauer spectroscopic study. *Appl. Catal. B* **164**, 407-419, (2015).
48 Fanning, P. E. & Vannice, M. A. A DRIFTS study of Cu-ZSM-5 prior to and during its use for N_2O decomposition. *J. Catal.* **207**, 166-182, (2002).
49 Dedecek, J., Balgova, V., Pashkova, V., Klein, P. & Wichterlova, B. Synthesis of ZSM-5 Zeolites with Defined Distribution of Al Atoms in the Framework and Multinuclear MAS NMR Analysis of the Control of Al Distribution. *Chem. Mater.* **24**, 3231-3239, (2012).
50 Borfecchia, E., Lomachenko, K. A., Giordanino, F., Falsig, H., Beato, P., Soldatov, A. V., Bordiga, S. & Lamberti, C. Revisiting the nature of Cu sites in the activated Cu-SSZ-13 catalyst for SCR reaction. *Chem. Sci.* **6**, 548-563, (2015).
51 Paolucci, C. K., I. Parekh, A. A. Li, S. C. Shih, A. J. Li, H. Di Iorio, J. R. Albarracin-Caballero, J. D. Yezerets, A. Miller, J. T. Delgass, W. N. Ribeiro, F. H. Schneider, W. F. Gounder, R. Dynamic multinuclear sites formed by mobilized copper ions in NOx selective catalytic reduction. *Science* **357**, 898-903, (2017).
52 Latimer, A. A. K., A. R. Aljama, H. Montoya, J. H. Yoo, J. S. Tsai, C. Abild-Pedersen, F. Studt, F. Norskov, J. K. Understanding trends in C-H bond activation in heterogeneous catalysis. *Nat. Mater.* **16**, 225-229, (2017).
53 Kulkarni, A. R., Zhao, Z. J., Siahrostami, S., Norskov, J. K. & Studt, F. Cation-exchanged zeolites for the selective oxidation of methane to methanol. *Catal. Sci. Technol.* **8**, 114-123, (2018).

54 Zhao, Z. J., Kulkarni, A., Vilella, L., Norskov, J. K. & Studt, F. Theoretical Insights into the Selective Oxidation of Methane to Methanol in Copper-Exchanged Mordenite. *ACS Catal.* **6**, 3760-3766, (2016).
55 Mahyuddin, M. H., Staykov, A., Shiota, Y., Miyanishi, M. & Yoshizawa, K. Roles of Zeolite Confinement and Cu-O-Cu Angle on the Direct Conversion of Methane to Methanol by $[Cu_2(\mu\text{-}O)]^{2+}$-Exchanged AEI, CHA, AFX, and MFI Zeolites. *ACS Catal.* **7**, 3741-3751, (2017).
56 Mahyuddin, M. H., Staykov, A., Shiota, Y. & Yoshizawa, K. Direct Conversion of Methane to Methanol by Metal-Exchanged ZSM-5 Zeolite (Metal = Fe, Co, Ni, Cu). *ACS Catal.* **6**, 8321-8331, (2016).
57 Mahyuddin, M. H., Tanaka, T., Shiota, Y., Staykov, A. & Yoshizawa, K. Methane Partial Oxidation over $[Cu_2(\mu\text{-}O)]^{2+}$ and $[Cu_3(\mu\text{-}O)_3]^{2+}$ Active Species in Large-Pore Zeolites. *ACS Catal.* **8**, 1500-1509, (2018).
58 Larsen, A. H. M., J. J. Blomqvist, J. Castelli, I. E. Christensen, R. Dulak, M. Friis, J. Groves, M. N. Hammer, B. Hargus, C. Hermes, E. D. Jennings, P. C. Jensen, P. B. Kermode, J. Kitchin, J. R. Kolsbjerg, E. L. Kubal, J. Kaasbjerg, K. Lysgaard, S. Maronsson, J. B. Maxson, T. Olsen, T. Pastewka, L. Peterson, A. Rostgaard, C. Schiotz, J. Schutt, O. Strange, M. Thygesen, K. S. Vegge, T. Vilhelmsen, L. Walter, M. Zeng, Z. H. Jacobsen, K. W. The atomic simulation environment-a Python library for working with atoms. *J. Phys.: Condens. Matter.* **29**, (2017).
59 Knott, B. C., Nimlos, C. T., Robichaud, D. J., Nimlos, M. R., Kim, S. & Gounder, R. Consideration of the Aluminum Distribution in Zeolites in Theoretical and Experimental Catalysis Research. *ACS Catal.* **8**, 770-784, (2018).
60 Wang, S., He, Y., Jiao, W. Y., Wang, J. G. & Fan, W. B. Recent experimental and theoretical studies on Al siting/acid site distribution in zeolite framework. *Curr. Opin. Chem. Eng.* **23**, 146-154, (2019).
61 Dedecek, J., Tabor, E. & Sklenak, S. Tuning the Aluminum Distribution in Zeolites to Increase their Performance in Acid-Catalyzed Reactions. *Chemsuschem* **12**, 556-576, (2019).
62 Itadani, A. S., H. Tanaka, M. Mori, T. Nagao, M. Kuroda, Y. New information related to the adsorption model of N_2 on CuMFI at room temperature. *J. Phys. Chem. C* **111**, 16701-16705, (2007).
63 Henriques, C., Ribeiro, M. F., Abreu, C., Murphy, D. M., Poignant, F., Saussey, J. & Lavalley, J. C. An FT-IR study of NO adsorption over Cu-exchanged MFI catalysts: Effect of Si/Al ratio, copper loading and catalyst pre-treatment. *Appl. Catal. B* **16**, 79-95, (1998).
64 Kosinov, N., Liu, C., Hensen, E. J. M. & Pidko, E. A. Engineering of Transition Metal Catalysts Confined in Zeolites. *Chem. Mater.* **30**, 3177-3198, (2018).
65 Agarwal, N. F., S. J. McVicker, R. U. Althahban, S. M. Dimitratos, N. He, Q. Morgan, D. J. Jenkins, R. L. Willock, D. J. Taylor, S. H. Kiely, C. J. Hutchings, G. J. Aqueous Au-Pd colloids catalyze selective CH_4 oxidation to CH_3OH with O_2 under mild conditions. *Science* **358**, 223-226, (2017).
66 Vanelderen, P. S., B. E. R. Tsai, M. L. Hadt, R. G. Vancauwenbergh, J. Coussens, O. Schoonheydt, R. A. Sels, B. F. Solomon, E. I. Spectroscopic Definition of the Copper Active Sites in Mordenite: Selective Methane Oxidation. *J. Am. Chem. Soc.* **137**, 6383-6392, (2015).
67 Morpurgo, S., Moretti, G. & Bossa, M. A computational study on the mechanism of NO decomposition catalyzed by Cu-ZSM-5: A comparison between single and dimeric Cu+ active sites. *J. Mole. Catal. a Chem.* **358**, 134-144, (2012).
68 Morpurgo, S. A DFT study on the mechanism of NO decomposition catalyzed by short-distance Cu(I) pairs in Cu-ZSM-5. *Mole. Catal.* **434**, 96-105, (2017).
69 Schneider, W. F., Hass, K. C., Ramprasad, R. & Adams, J. B. First-principles analysis of elementary steps in the catalytic decomposition of NO by Cu-exchanged zeolites. *J. Phys. Chem. B* **101**, 4353-4357, (1997).
70 Sajith, P. K., Shiota, Y. & Yoshizawa, K. Role of Acidic Proton in the Decomposition of NO over Dimeric Cu(I) Active Sites in Cu-ZSM-5 Catalyst: A QM/MM Study. *ACS CataL.* **4**, 2075-2085, (2014).

71 Ganemi, B., Bjornbom, E. & Paul, J. Conversion and in situ FTIR studies of direct NO decomposition over Cu-ZSM5. *Appl. Catal. B.* **17**, 293-311, (1998).
72 Hadjiivanov, K. I. Identification of neutral and charged N_xO_y surface species by IR spectroscopy. *Catal. Rev.* **42**, 71-144, (2000).
73 Izquierdo, R., Rodriguez, L. J., Anez, R. & Sierraalta, A. Direct catalytic decomposition of NO with Cu-ZSM-5: A DFT-ONIOM study. *J. Mole. Catal. A Chem.* **348**, 55-62, (2011).
74 Kuroda, Y., Kumashiro, R., Yoshimoto, T. & Nagao, M. Characterization of active sites on copper ion-exchanged ZSM-5-type zeolite for NO decomposition reaction. *Phys. Chem. Chem. Phys.* **1**, 649-656, (1999).
75 Rice, M. J., Chakraborty, A. K. & Bell, A. T. Al next nearest neighbor, ring occupation, and proximity statistics in ZSM-5. *J. Catal.* **186**, 222-227, (1999).
76 Lee, D. K. Thermodynamic features of the Cu-ZSM-5 catalyzed NO decomposition reaction. *Korean. J. Chem. Eng.* **23**, 547-554, (2006).
77 Aranovich, G. L. D., M. D. Phase loops in density-functional-theory calculations of adsorption in nanoscale pores. *Phys. Rev. E* **60**, 5552-5560, (1999).
78 Aranovich, G. L. & Donohue, M. D. Adsorption compression: An important new aspect of adsorption behavior and capillarity. *Langmuir* **19**, 2722-2735, (2003).
79 Sumanatrakul, P., Abaza, S., Aranovich, G. L., Sangwichien, C. & Donohue, M. D. Pattern of adsorption isotherms in Ono-Kondo coordinates. *J. Colloid Interface Sci.* **368**, 427-433, (2012).
80 Smeets, P. J. G., M. H. van Teeffelen, R. M. Leeman, H. Hensen, E. J. M. Schoonheydt, R. A. Direct NO and N_2O decomposition and NO-assisted N_2O decomposition over Cu-zeolites: Elucidating the influence of the Cu-Cu distance on oxygen migration. *J. Catal.* **245**, 358-368, (2007).
81 Beale, A. M. G., F. Lezcano-Gonzalez, I. Peden, C. H. F. Szanyi, J. Recent advances in automotive catalysis for NOx emission control by small-pore microporous materials. *Chem. Soc. Rev.* **44**, 7371-7405, (2015).
82 Teraishi, K. I., M. Irisawa, J. Kume, M. Takahashi, Y. Nakano, T. Nakamura, H. Miyamoto, A. Active site structure of Cu/ZSM-5: Computational study. *J. Phys. Chem. B* **101**, 8079-8085, (1997).
83 Schay, Z., Knozinger, H., Guczi, L. & Pal-Borbely, G. On the mechanism of NO decomposition on Cu-ZSM-5 catalysts. *Appl. Catal. B* **18**, 263-271, (1998).
84 Iwamoto, M. Y., H. Tanda, K. Mizuno, N. Mine, Y. Kagawa, S. Removal of Nitrogen Monoxide through a Novel Catalytic Process .1. Decomposition on Excessively Copper-Ion Exchanged ZSM-5 Zeolites. *J. Phys. Chem.* **95**, 3727-3730, (1991).
85 Sushkevich, V. L. P., D. Ranocchiari, M. van Bokhoven, J. A. Selective anaerobic oxidation of methane enables direct synthesis of methanol. *Science* **356**, 523-527, (2017).
86 Li, Y. L., L. Yu, J. H. Applications of Zeolites in Sustainable Chemistry. *Chem* **3**, 928-949, (2017).
87 Dusselier, M. & Davis, M. E. Small-Pore Zeolites: Synthesis and Catalysis. *Chem. Rev.* **118**, 5265-5329, (2018).
88 Verma, A. A. B., S. A. Anggara, T. Paolucci, C. Parekh, A. A. Kamasamudram, K. Yezerets, A. Miller, J. T. Delgass, W. N. Schneider, W. F. Ribeiro, F. H. NO oxidation: A probe reaction on Cu-SSZ-13. *J. Catal.* **312**, 179-190, (2014).
89 Godiksen, A. V., P. Rasmussen, S. Mossin, S. Identification and Quantification of Copper Sites in Zeolites by Electron Paramagnetic Resonance Spectroscopy. *Top. Catal.* **60**, 13-29, (2017).
90 Pappas, D. K. M., A. Dyballa, M. Kvande, K. Teketel, S. Lomachenko, K. A. Baran, R. Glatzel, P. Arstad, B. Berlier, G. Lamberti, C. Bordiga, S. Olsbye, U. Svelle, S. Beato, P. Borfecchia, E. The Nuclearity of the Active Site for Methane to Methanol Conversion in Cu-Mordenite: A Quantitative Assessment. *J. Am. Chem. Soc.* **140**, 15270-15278, (2018).

91 Narsimhan, K., Iyoki, K., Dinh, K. & Roman-Leshkov, Y. Catalytic Oxidation of Methane into Methanol over Copper-Exchanged Zeolites with Oxygen at Low Temperature. *ACS Cent. Sci.* **2**, 424-429, (2016).

92 Tomkins, P. *et al.* Isothermal Cyclic Conversion of Methane into Methanol over Copper-Exchanged Zeolite at Low Temperature. *Angew.Chem. Int. Ed.* **55**, 5467-5471, (2016).

93 Yumura, T., Hirose, Y., Wakasugi, T., Kuroda, Y. & Kobayashi, H. Roles of Water Molecules in Modulating the Reactivity of Dioxygen-Bound Cu-ZSM-5 toward Methane: A Theoretical Prediction. *ACS Catal.* **6**, 2487-2495, (2016).

Figures

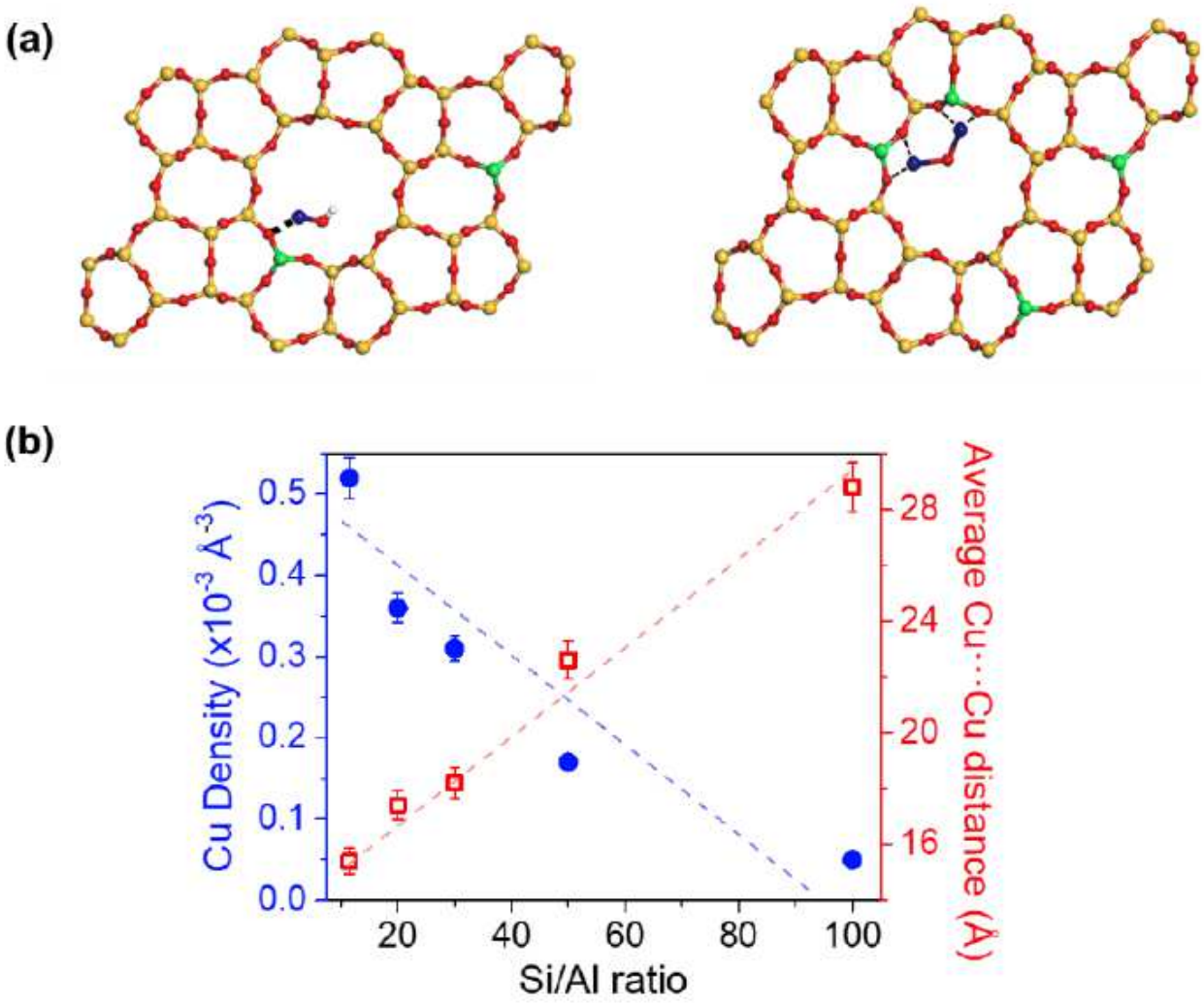

Figure 1

Graphical illustration and characterization of Cu sites in ZSM5. (a) Geometric models of a Cu monomer site (left) and an oxygen bridged Cu dimer site (right) in Cu-ZSM5. (b) Dependence of Cu density (per unit volume of the zeolite pore) and average Cu-Cu distance on Si/Al ratio in Cu-ZSM5.

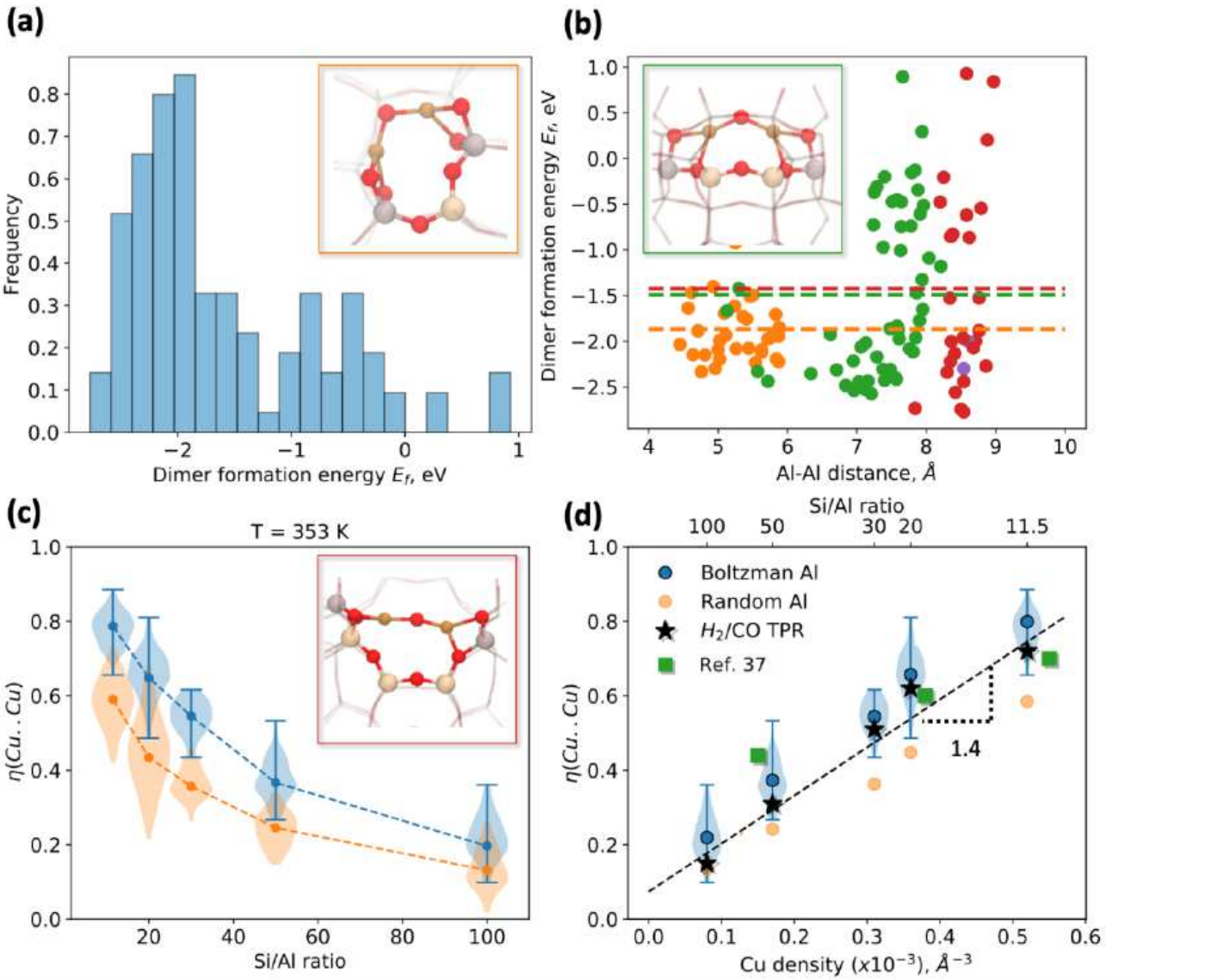

Figure 2

(a) Histogram showing the distribution of dimer formation energies (Ef) for all possible [CuOCu]2+ dimers in MFI. (b) Ef at different Al-Al distances and #Si atoms between the 2Al atoms: 1T (orange), 2T (green), 3T (red) and 4T (purple); the dotted lines show the average Ef. (c) Fraction of Cu dimers in MFI, η(Cu..Cu) at 80 °C assuming a Boltzmann-weighted (blue) and random (orange) distribution of Al atoms. (d) Linear relationship between the Cu dimer fraction derived from DFT calculations (blue) and TPR measurements (black stars) with Cu density and Si/Al ratio. The experimental data from Ref. 37 (green squares) is consistent with our computational predictions. The insets in (a), (b) and (c) show the structures of the most favorable 1T, 2T and 3T dimer configuration in MFI.

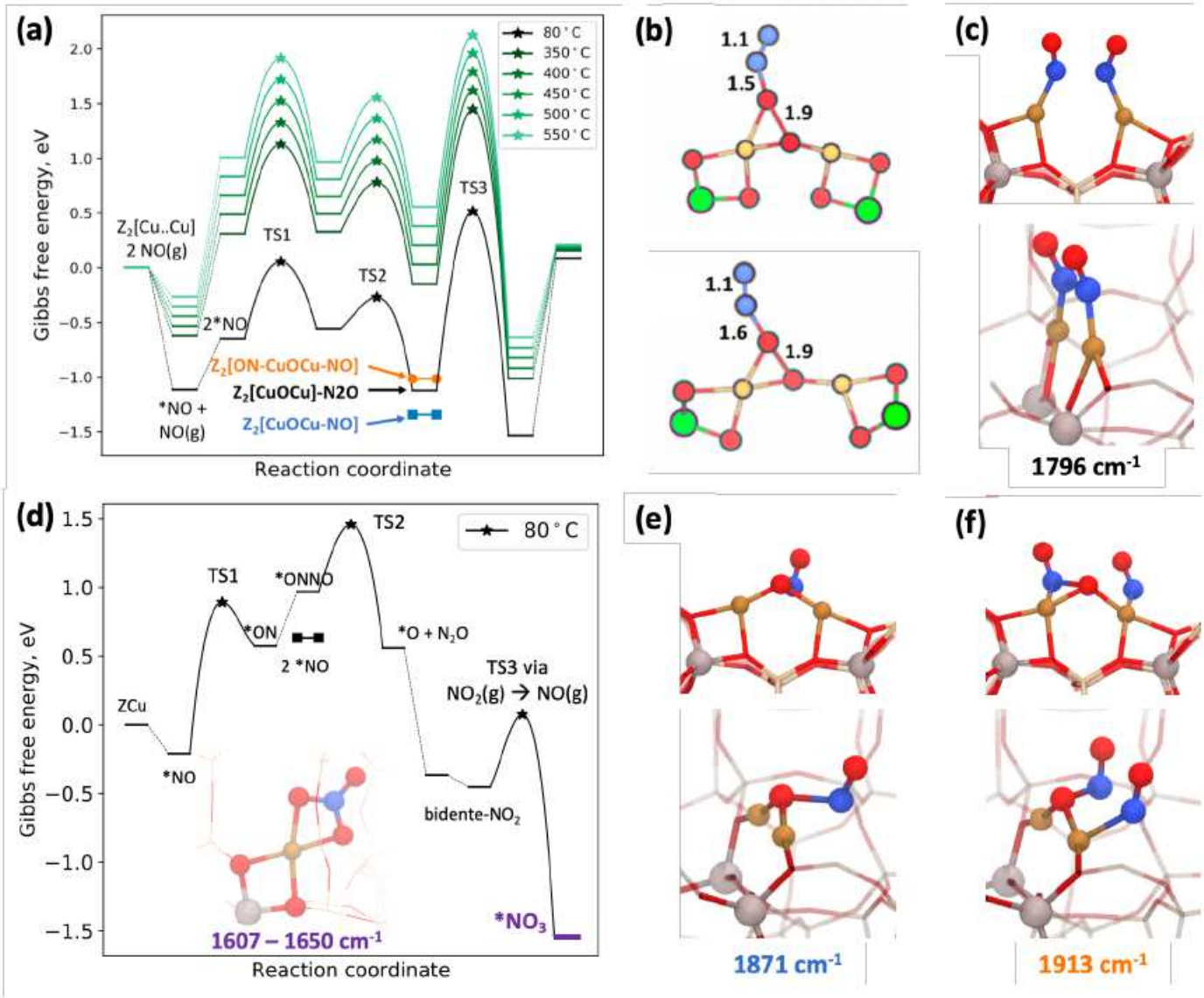

Figure 3

(a) DFT calculated free energy diagrams at various temperatures for NO decomposition by Cu dimers in 1T-MFI; free energies of one and two NO bound dimers are shown in orange and blue, respectively. (b) The transition states for N2O decomposition for 1T (upper) and 2T (lower) models (Red: O, Blue: N, Yellow: Cu, Green: Al), (c) – (f) structure model and vibrational frequencies for [(ON)Cu+□□□Cu+(NO)], [Cu-NO3]+, NO-[Cu-O-Cu]2+ and [(NO)Cu-O-Cu(NO)]2+, respectively (Red: O, Blue: N, Yellow: Cu, Gray: Al). The free energy diagram for the isolated-Cu site is shown in (d) at 80 °C.

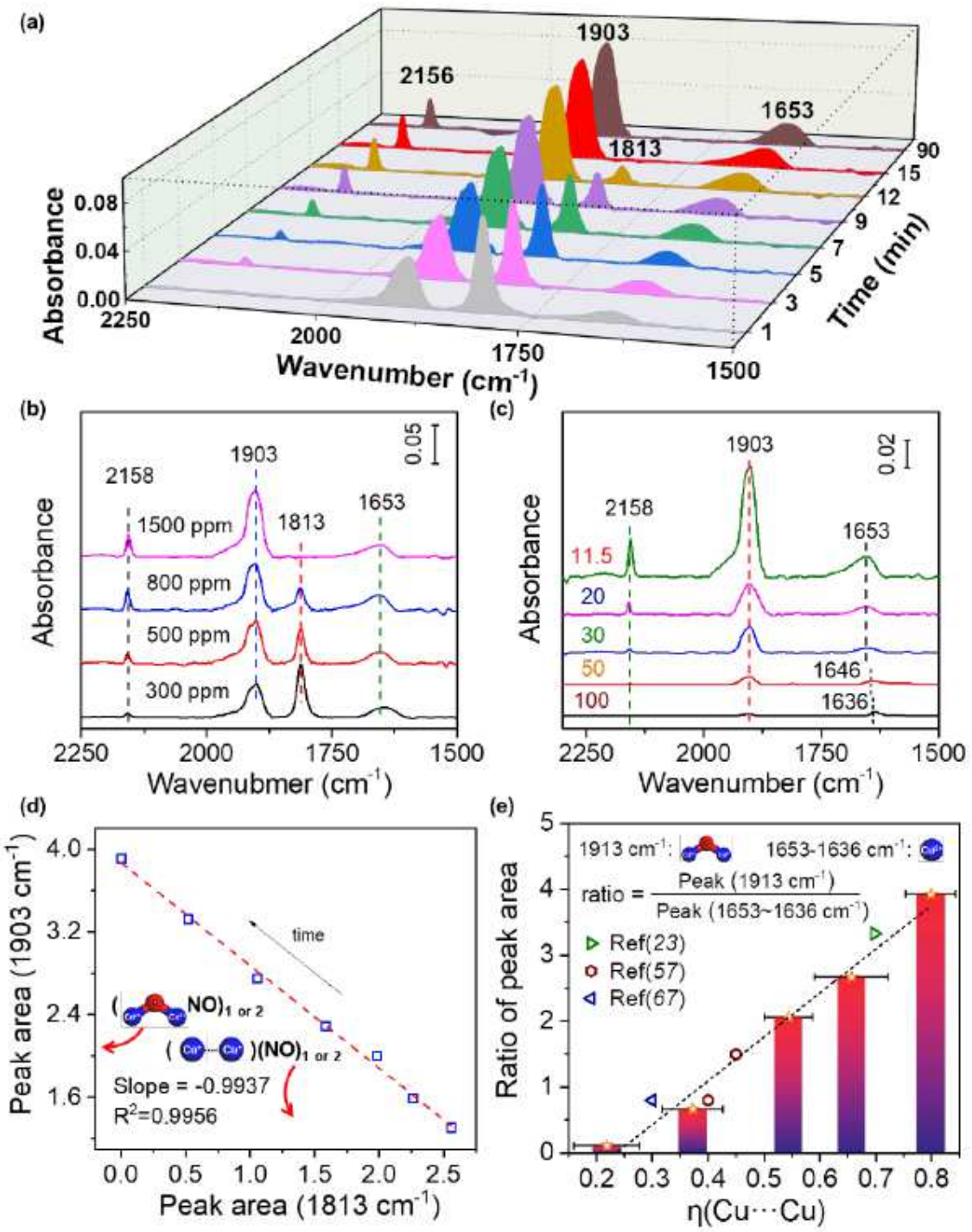

Figure 4

Characterization and quantification of Cu dimers in Cu-ZSM5 zeolites. (a) Time dependence DRIFTs of NO isothermal adsorption at 80 °C on Cu-ZSM5-11.5 at 1500 ppm. (b) Pressure dependence DRIFTs of NO isothermal adsorption at 80 °C on Cu-ZSM5-11.5 at 15 min. (c) DRIFTs of NO isothermal adsorption at 80 °C on Cu-ZSM5 with different Si/Al ratios at 1500 ppm and 15 min. (d) Correlation of integrated peak areas of 1903 cm-1 peak and 1813 cm-1 peak in DRIFT spectra of NO isothermal adsorption at 80

°C and 1500 ppm on Cu-ZSM5-11.5 at different times. (e) Correlation of area ratios of 1903 cm-1 peak and 1813 cm-1 peak in DRIFT spectra of NO isothermal adsorption at 80 °C on Cu-ZSM5 and Cu dimer fraction from DFT calculation and TPR measurements.

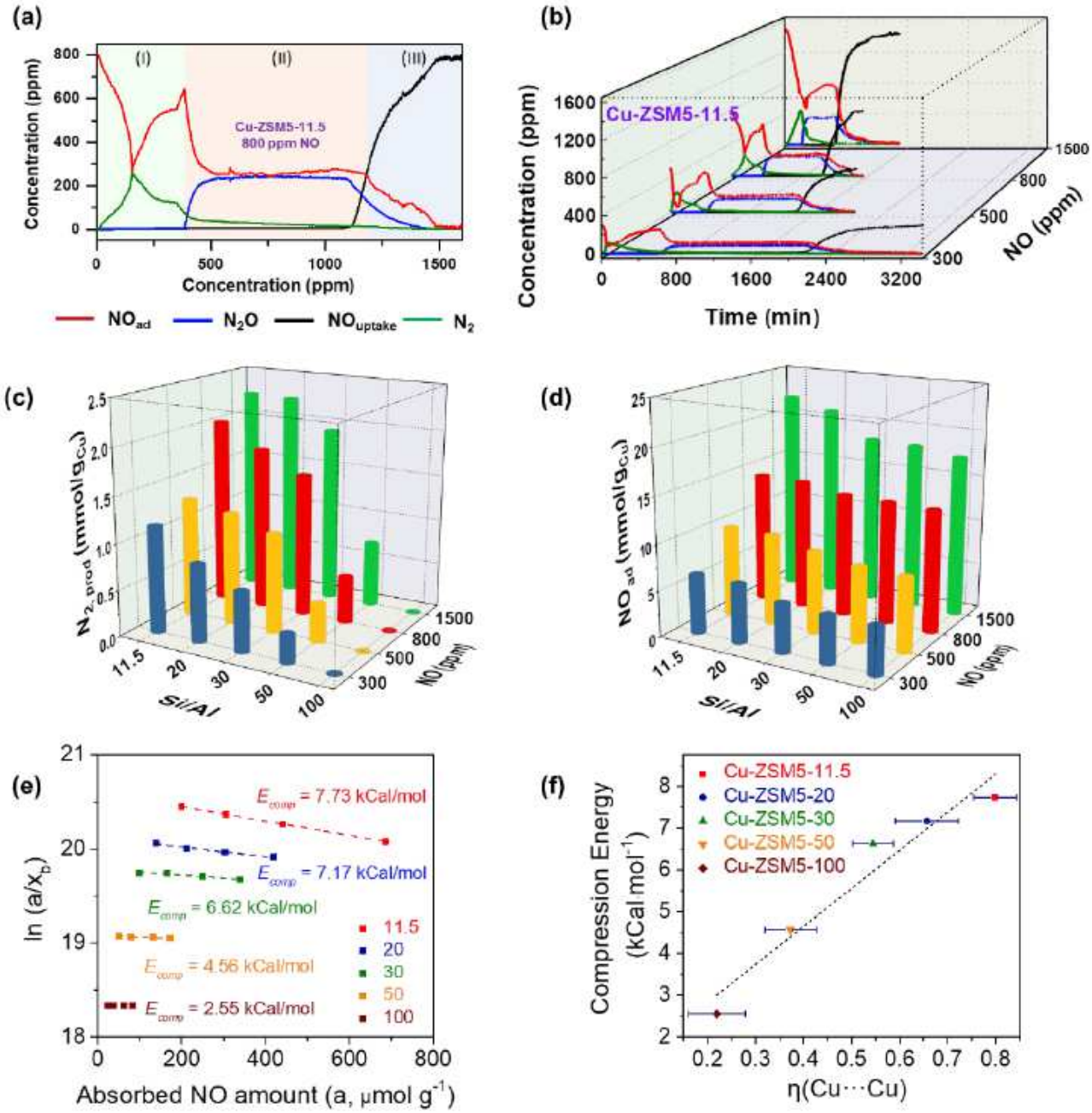

Figure 5

NO Isothermal adsorption profiles. (NOad: red, N2,prod: green, N2Oprod: blue, NOuptake: black) (a) Time dependent profiles of outlet concentrations of NO, N2O and N2 during NO isothermal adsorptions at 80 °C with 800 ppm of NO on Cu-ZSM5-11.5. (b) Time dependent plot of outlet concentrations of NO, N2O and N2 during NO isothermal adsorptions at 80 °C with different pressures of NO for Cu-ZSM5-11.5. (c) plot

of N2 production per Cu site during NO isothermal adsorption at different NO pressures on the five Cu-ZSM5. (d) plots of adsorbed NO per Cu site during NO isothermal adsorption at different NO pressures on Cu-ZSM5 zeolites. (e) Ono-Kondo plots for compression energies of Cu-ZSM5 zeolites. (f) Correlation of calculated compression energy and average Cu-Cu distance in Cu-ZSM5 zeolites.

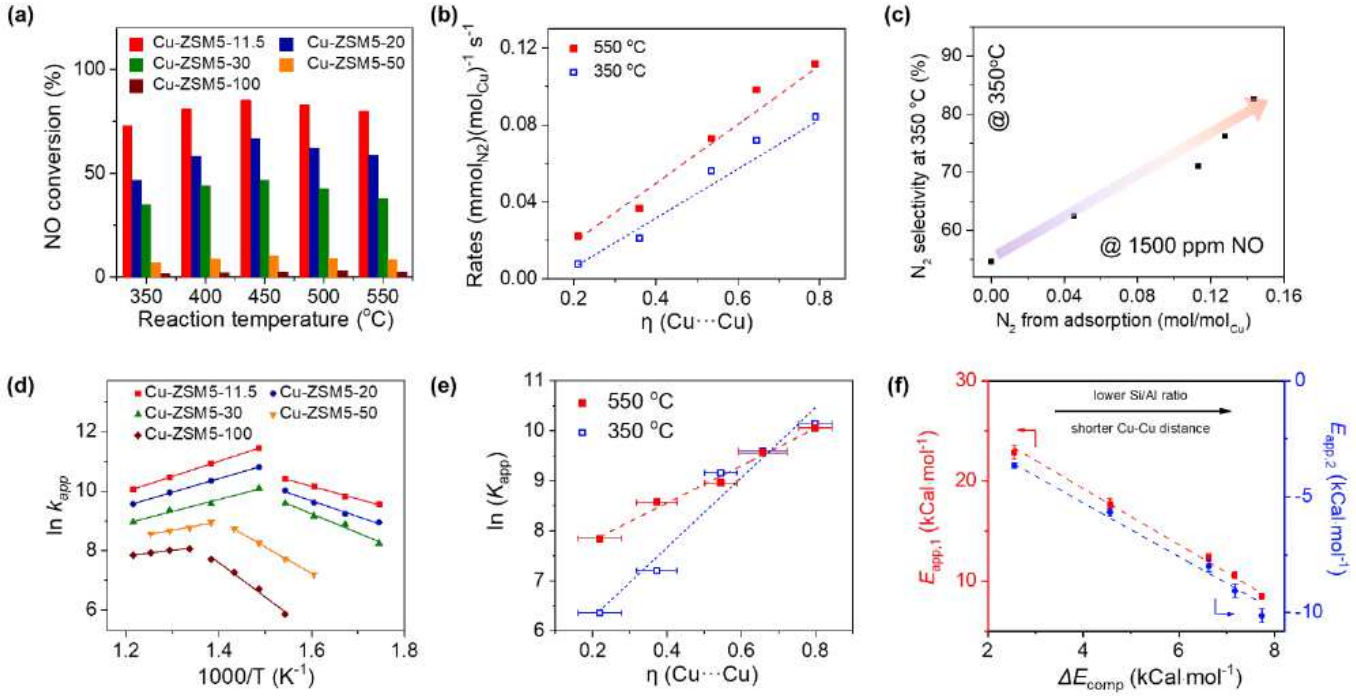

Figure 6

Catalytic performance and Kinetics of NO Decomposition. (a) Conversions of NO over different Cu-ZSM5. (b) Correlations between rates of N2 at 350, 550 °Cand fractions of Cu dimers. (c) Trends of N2 selectivity at 350 depending on N2 production during NO isothermal adsorptions at 80 °C with 1500 ppm of NO on Cu-ZSM5 zeolites. (d) Arrhenius plots for rate constants vs 1/T. (e) Correlations between ln(Kapp) at 350, 550 °C and fractions of Cu dimers fractions. (f) Correlation of apparent activation energies at low temperatures (red, left) and at high temperatures (blue, right) with compression energy derived from Ono-Kondo coordinates.

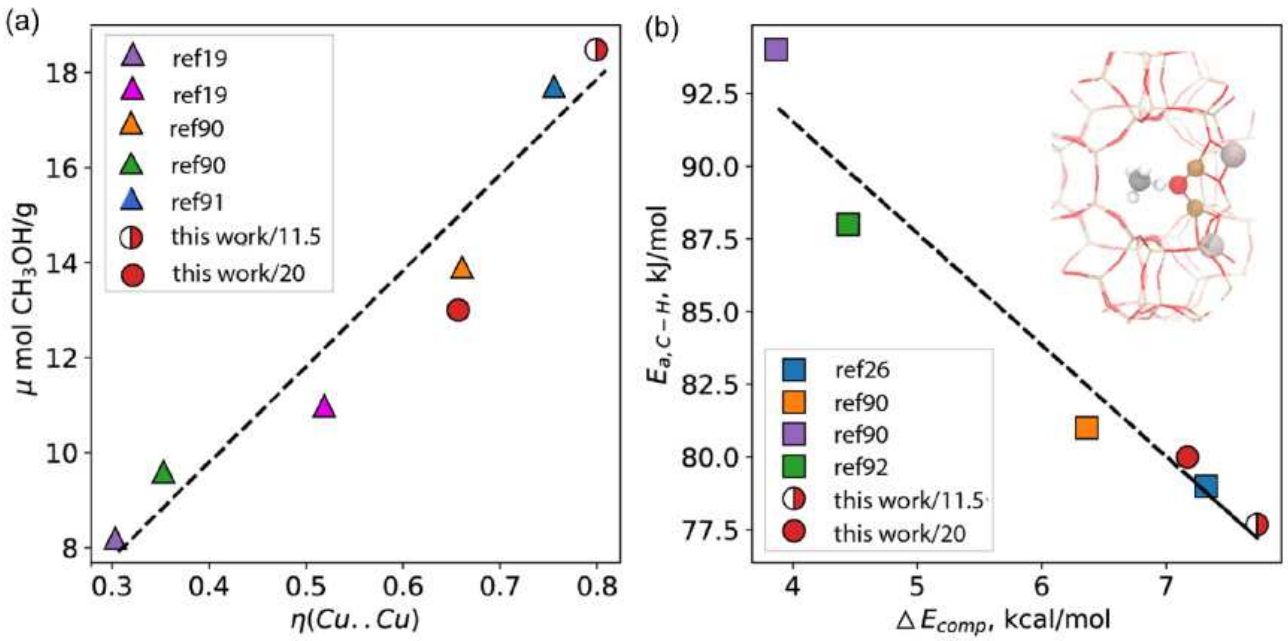

Figure 7

Catalytic study of methane to methanol by using Cu-ZSM5 from the literature and this work. (a) Correlations between the methanol yields with Cu dimers fractions; (b) Correlation of apparent methane activation energies with compression energies. Hereby the Cu dimers fractions and compression energies are derived by fitting the Cu densities from literature into the scaling established in Figure 2d and Figure 5f.

Supplementary Files

This is a list of supplementary files associated with this preprint. Click to download.

- 2020820CuZSM5DeNOxSI.pdf